







The nature of insoluble organic matter in Sutter’s Mill and Murchison carbonaceous chondrites: Testing the effect of x-ray computed tomography and exploring parent body organic molecular evolution

George D. CODY ^{1*}, Conel M. O’D. ALEXANDER ¹, Dionysis I. FOUSTOUKOS¹,
Henner BUSEMANN ², Scott ECKLEY ³, Aaron S. BURTON⁴, Eve L. BERGER⁴,
Michel NUEVO⁵, Scott A. SANDFORD⁵, Daniel P. GLAVIN ⁶, Jason P. DWORKIN ⁶,
Harold C. CONNOLLY JR^{7,8,9}, and Dante S. LAURETTA⁸

¹Earth and Planets Laboratory, Carnegie Institution for Science, Washington, DC, USA

²ETH Zurich, Institute of Geochemistry and Petrology, Zurich, Switzerland

³Jacobs Technology, NASA Johnson Space Center, Houston, Texas, USA

⁴NASA Johnson Space Center, Houston, Texas, USA

⁵NASA Ames Research Center, Moffett Field, California, USA

⁶NASA Goddard Space Flight Center, Greenbelt, Maryland, USA

⁷Department of Geology, School of Earth and Environment, Rowan University, Glassboro, New Jersey, USA

⁸Lunar and Planetary Laboratory, University of Arizona, Tucson, Arizona, USA

⁹Department of Earth and Planetary Science, American Museum of Natural History, New York, New York, USA

*Correspondence

George D. Cody, Earth and Planets Laboratory, Carnegie Institution for Science, Washington, DC 20015, USA.

Email: gcody@arnegiescience.edu

(Received 20 July 2023; revision accepted 10 October 2023)

Abstract—This study analyzed samples of the Murchison and Sutter’s Mill carbonaceous chondrite meteorites in support of the future analysis of samples returned from the asteroid (10155) Bennu by the OSIRIS-REx (Origins, Spectral Interpretation, Resource Identification, and Security–Regolith Explorer) mission. Focusing specifically on the insoluble organic matter (IOM), this study establishes that a total of 1.3 g of bulk sample from a single chondritic meteorite are sufficient to obtain a wide range of cosmochemical information, including light element analysis (H, C, and N), isotopic analysis (D/H, ¹³C/¹²C, and ¹⁵N/¹⁴N), and x-ray fluorescence spectroscopy for major elemental abundances. IOM isolated from the bulk meteorite samples was analyzed by light element and isotopic analysis as described above, ¹H and ¹³C solid-state nuclear magnetic resonance spectroscopy, Raman spectroscopy, and complete noble gas analyses (abundances and isotopes). The samples studied included a pair from Murchison (CM2), one of which had been irradiated with high-energy x-rays in the course of computed tomographic imaging. No differences between the irradiated and non-irradiated Murchison samples were observed in the many different chemical and spectroscopic analyses, indicating that any x-ray-derived sample damage is below levels of detection. Elemental, isotopic, and molecular spectroscopic data derived from IOM isolated from the Sutter’s Mill sample reveals evidence that this meteorite falls into the class of heated CM chondrites.

INTRODUCTION

The OSIRIS-REx (Origins, Spectral Interpretation, Resource Identification, and Security–Regolith Explorer) mission will deliver samples of regolith in September 2023

from (101955) Bennu, a carbonaceous B-type asteroid similar to aqueously altered CI- and CM-type chondrites (Hamilton et al., 2019). Carbonaceous chondrites are known to contain considerable organic matter, predominantly in the form of an insoluble organic

macromolecular phase (insoluble organic matter, IOM, at ~2 wt%, Alexander et al., 2007) and a complex suite of soluble organic compounds (Glavin et al., 2018). In preparation for the analysis of returned Bennu samples, we focused on studying the IOM from previously studied carbonaceous chondrites acquired as meteorite falls and finds. This study verifies the techniques we will use to provide elemental, isotopic, and molecular spectroscopic insight into a major reservoir of Bennu's organic matter and enable us to place Bennu in context with the broader meteorite collection.

In preparation for our role in preliminary examination of IOM isolated from returned Bennu samples, the OSIRIS-REx mission required proof of stated analytical capabilities using selected ~1 g bulk samples from two carbonaceous chondrites: Murchison, a CM2 (split into subsamples A and B) and Sutter's Mill, an ungrouped C type chondrite that exhibits similarities to CMs (Jenniskens et al., 2012).

One major task in the preparations for Bennu sample analysis was to test whether x-ray computed tomography (XCT) could have negative (destructive) effects on organic matter contained within the samples. Toward this end, one of the two Murchison bulk samples (A or B) was subjected to XCT; the other sample was a control. During organics analyses, the identity of the irradiated sample was not provided to the analysts. Upon completion of the organics analyses, it was revealed that the Murchison B sample was the irradiated sample. The XCT was performed at NASA Johnson Space Center (JSC) and employed an unfiltered polychromatic x-ray beam up to 160 keV that subjected the Murchison B sample to a radiation dose of ~180 Gy. Details of the Murchison meteorite processing procedure and the XCT imaging experiment are reported in Glavin et al. (2023).

Our investigation focused on three primary goals. The first was to obtain H, C, and N elemental and isotopic (D/H, $^{13}\text{C}/^{12}\text{C}$, and $^{15}\text{N}/^{14}\text{N}$) compositions of the bulk meteorite samples by employing elemental analysis— isotope ratio mass spectrometry (EA-IRMS). A second goal involved demonstrating that isolating IOM from the meteorites can be achieved efficiently and reproducibly using the CsF-HF method (Alexander et al., 2007). A third goal involved obtaining the H, C, and N elemental and isotopic compositions of the IOM isolates, as well as their molecular compositions, by employing-IRMS, ^1H , and ^{13}C solid-state nuclear magnetic resonance (NMR) spectroscopy and Raman vibrational spectroscopy. Bulk samples were also analyzed by x-ray fluorescence (XRF) to determine the concentrations of major and trace elements. XRF analysis was performed on some unprocessed bulk powders after all the other analytical work was completed. Following these analyses, portions of the isolated IOM samples were then transferred to other OSIRIS-REx-

affiliated laboratories for noble gas and secondary ion mass spectrometry (SIMS) measurements. The results of the noble gas studies are included in this manuscript; the SIMS measurements will be published separately.

The preparations for Bennu sample return afforded an opportunity to analyze a new sample of Murchison (USNM 5453,1) for intra-sample variability through comparison with previous work on another Murchison sample (Alexander et al., 2007; Cody et al., 2002), as well as to perform new measurements on Sutter's Mill (Jenniskens et al., 2012). Whereas C and N elemental and isotopic abundances for Sutter's Mill IOM have been reported previously (Pizzarello et al., 2013), to our knowledge, the H/C and δD of its IOM have not been published. Similarly, while both ^1H and ^{13}C solid-state NMR spectra have been reported previously for Sutter's Mill IOM (Pizzarello et al., 2013), the quality of these published spectra was insufficient (largely due to poor signal strength, poor choice of key NMR parameters, and bad spectral phasing) to provide the information necessary to characterize the Sutter's Mill IOM molecular structure and place it in context with the structures of other well-characterized chondritic IOM samples (Alexander et al., 2017; Cody & Alexander, 2005; Herd et al., 2011; Yabuta et al., 2010).

MATERIALS AND METHODS

Samples

The Murchison sample (USNM 5453,1) was provided by the Smithsonian Institution's National Museum of Natural History. The OSIRIS-REx project provided two Sutter's Mill samples (UA 2537 and UA 2532,2), sourced from Stones 1 (SM1) and 8 (SM8), respectively (Jenniskens et al., 2012), that had not been previously analyzed. The Murchison and Sutter's Mill samples were prepared at NASA JSC by Arron Burton and Eve Berger, by grinding (by hand) each meteorite separately in an agate mortar and pestle, with the Murchison sample being split into two samples, A and B, and the Sutter's Mill samples (SM1 and SM8) were combined into a single sample. For Murchison, we were provided 1.3300 g of A and 1.3550 g of B, of which 1.2188 and 1.19919 g, respectively, were used for IOM isolation. The Sutter's Mill sample provided to us was 1.1899 g, of which 1.0734 g was used for IOM isolation. Roughly 100 mg of each bulk sample was retained for bulk analyses, including EA-IRMS and XRF.

Included in the present study for the purpose of comparison are IOM that were isolated previously from the Pecora Escarpment (PCA) 91008 and Wisconsin Range (WIS) 91600 meteorites where they were analyzed for the elemental abundances and H, C, and N stable

isotope concentrations (Alexander et al., 2007) and later with ^{13}C solid-state NMR (Yabuta et al., 2010).

Aluminum 4×4 mm plates (prepared at NASA GSFC by Jason Dworkin) were also analyzed as proxies to rehearse the analytical protocols for determining the background C and N elemental and isotopic abundances of witness plates mounted on OSIRIS-REx's sample collection mechanism and sample return capsule. These aluminum plates were deployed in an aluminum foil tray placed at the back of the HEPA flow bench where the Murchison and Sutter's Mill samples were processed at NASA JSC.

Isolation of IOM

The isolation of IOM from bulk meteorite samples was performed at the Earth and Planets Laboratory by Conel Alexander using the CsF-HF method described in Alexander et al. (2007). First, the powdered meteorites samples were leached with 2 N HCl, followed by rinsing with MilliQ water and dioxane. The samples were then shaken in the presence of two immiscible liquids, an aqueous CsF-HF solution ($1.6\text{--}1.7 \text{ g cc}^{-1}$) and dioxane. When shaken and centrifuged, the IOM is liberated from its mineral matrix and collects at the interface of the CsF-HF solution and the dioxane, while the denser minerals sink to the bottom. After centrifugation, the IOM was pipetted off. Repeated cycles of shaking, centrifugation, and pipetting of IOM were conducted until significant release of IOM ceased. The high-density material was then rinsed multiple times in 2 N HCl, then Milli-Q water and dioxane and finally CsF-HF solution to ensure complete IOM extraction. The IOM isolate was rinsed with 2 N HCl several times followed by Milli-Q water and dioxane, before being dried down at $<30\text{--}50^\circ\text{C}$. There was no specific attempt to remove soluble organic material. However, the repeated washing with aqueous solutions and dioxane should have effectively removed most soluble organic compounds known to be present in chondrites. Sulfides can survive this process; to remove them, the IOM is left in air for several days and then rinsed with 2 N HCl, Milli-Q water, and dioxane. This process is repeated several times until there is no significant mass loss and the acid solution remains clear. The entire IOM purification process requires several weeks.

Elemental Analysis of Bulk Meteorites and IOM

The bulk H, C, and N elemental and isotopic analyses were performed at the Earth and Planets Laboratory by Dionysis Foustoukos using previously established protocols (Alexander et al., 2012, 2013; Foustoukos et al., 2021). For H, C, and N analyses, samples were weighed into Ag (for H; 2.1–3.6 mg) and Sn (for C and N; 7.8–

9.1 mg) capsules. The samples were stored in a desiccator for several days and reweighed to remove adsorbed atmospheric water. Prior to H analysis, the samples were placed in an autosampler and flushed with zero grade, dry He for 2 h to remove water absorbed from the atmosphere during the transfer from the desiccator to the autosampler.

The elemental and isotopic analyses were made with (i) a Thermo Scientific Delta V^{plus} mass spectrometer connected to a Carlo Erba (NA 2500) elemental analyzer (CE/EA) via a Conflo III interface for C and N analyses, and (ii) a Thermo Finnigan Delta Plus XL mass spectrometer connected to a Thermo Finnigan Thermal Conversion elemental analyzer (TC/EA) via a Conflo III interface for H analyses. The Conflo III interface facilitates the introduction of the N_2 and CO_2 reference gases for the N and C isotope analyses. In contrast, a dual inlet system facilitates the introduction of the H_2 reference gas for the H isotope analyses. A H_3^+ correction was determined and applied to the H measurements (Sessions, 2001). We used in-house standards to normalize and correct the data at regular intervals to monitor the accuracy and precision of the measured isotopic ratios and elemental compositions throughout the runs. These in-house standards, which included both gases and solid materials, have been calibrated against international (Standard Mean Ocean Water or SMOW, National Bureau of Standards-22, Pee Dee Belemnite, and air) and other certified standards from the Isoanalytical Laboratory, the U.S. Geological Survey, the National Bureau of Standards, and the Oztech Trading Company. The reported uncertainties for the elemental and isotopic analyses correspond to the highest 1σ deviations attained from either the replicate analyses of distinct subsamples or the internal standards. For the H analyses, replicate samples were analyzed sequentially to check for both sample heterogeneity and small memory effects that occur. Blanks were run before and after samples, again to reduce any memory effects. For example, the H abundances of the duplicate samples generally differed by $\leq 3\%$ of their absolute values, and the δD values differed by a median of 8‰ (the δ notation stands for the deviation of a sample ratio from a standard ratio in parts per thousand, $\delta = (R_{\text{smp}}/R_{\text{std}} - 1) \times 1000$, and in this case $R = \text{D}/\text{H}$). There is no memory effect for C and N analyses, and the larger sample sizes ensured more representative sampling of the powders.

^1H and ^{13}C Solid-State NMR of IOM

Solid-state ^1H and ^{13}C -NMR experiments were performed at the Earth and Planets Laboratory by George Cody using a Chemagnetics 300 Infinity NMR at a magnetic field strength of 7.05 T (where the Larmor frequencies of ^1H and ^{13}C are ~ 300 and 75 MHz,

respectively). Given the small quantities of sample, ^1H - ^{13}C cross polarization (CP) NMR (employing an amplitude ramp on the ^{13}C channel) was performed to obtain ^{13}C -NMR data. Samples were loaded into a 5-mm diameter zirconia oxide rotor placed within the coil of a double resonance radio frequency (RF) probe. The key parameters for the CP measurements were magic angle sample spinning (MAS) at a frequency of 11.5 kHz, a 4 μs 90° excitation pulse on ^1H , using a ramped (variable amplitude pulse power, VA) ^{13}C spin-lock across the -1 (low frequency) sideband of the Hartman–Hahn match frequency, a 4.5 ms contact time (CT) optimized for VACPMAS NMR of IOM (Cody et al., 2002; Cody & Alexander, 2005), a recycle delay (RD) of 1 s, and with ^1H RF decoupling at a frequency of 63.5 kHz. A total of 80,000 transients were acquired and combined to produce the ^{13}C -NMR spectra. The ^{13}C -NMR spectra were referenced to tetramethyl silane (TMS) using a secondary reference compound (hexamethyl benzene). ^1H solid-state NMR was performed in 2.5 mm zirconia rotors in a moderately fast MAS, double resonance RF probe. The DEPTH background reduction pulse program was employed. Key parameters are: MAS = 22 kHz, ^1H 90° pulse width of 3 μs , and a RD of 1 s. A total of 80,000 transients were acquired and combined to produce the ^1H -NMR spectra. The ^1H -NMR spectra were referenced to TMS using hexamethyl benzene.

Synthesis of syn-IOM and Investigating Reduction of syn-IOM Carbonyls with Sodium Borohydride (NaBH_4)

The experimental synthesis and reduction of a chemical simulant of chondritic IOM, called syn-IOM, was performed at the Earth and Planets Laboratory by George Cody. Reactions involving formaldehyde in liquid water (Cody et al., 2011; Foustoukos et al., 2021; Kebukawa et al., 2013; Kebukawa & Cody, 2015) yield organic solids that are nearly identical to actual IOM at the functional group level. For this study, synthetic IOM was derived from glucose (equivalent to six formaldehyde molecules) in water through hydrocarbonization as follows. First, 170 mg of glucose was added to 1.5 mL of distilled water (this is within the range of composition of formaldehyde equivalents detected in interstellar ices). The solution was flame-sealed in a glass tube and heated in a convection oven at 250°C for exactly 7 h. Because the syn-IOM reaction generates considerable gas pressure (largely CO_2 and H_2) after heating the following protocol was performed for safety reasons. The glass tube was first placed in an -80°C freezer for several hours. The tube was then immersed in a dewar filled with liquid N_2 to freeze the predominantly CO_2 gas to solid. Wearing cryoprotective gloves and a face shield, the glass tube was scored with a stainless steel file and then split into two open halves. The

time taken for the open glass tube come to room temperature allowed for the effervescence, mostly CO_2 , to cease. The glass tube halves were then covered with perforated aluminum foil and refrozen at -80°C and freeze-dried for approximately 12 h. Once dried, the samples were weighed. The typical yield is approximately 50% of the starting weight of glucose.

Carbonyl reduction to alcohol of dry syn-IOM was performed in HPLC grade methanol using 70 mg of sodium borohydride (NaBH_4 ; Sigma-Aldrich) and 100 mg of syn-IOM powder (note: sodium borohydride is a dangerous and highly toxic compound that must be handled with considerable care and caution). The stirred reaction (proceeding in 22 mL capped vials) was performed for ~ 3 weeks (reduction in solution occurs fairly rapidly, but with solids, issues related to diffusion suggested that greater reaction time is necessary). The slurry was transferred to a 4-mL vial and 0.3 mL of 3 N HCl was added, followed by 10% HCl that initiates effervescence. After effervescence ceased, the sample vial was centrifuged at 2000 g for 20 min, the supernatant was pipetted off and an additional 10% HCl was added, followed by centrifugation. After three more cycles with distilled water, the solution remained clear, and the sample was again frozen at -80°C and freeze-dried. Evidence of partial reduction of carbonyls and carboxyl to alcohols was verified using ^{13}C VACPMAS NMR (see below in the solid-state NMR discussion).

Raman Vibrational Spectroscopy of IOM

The Raman spectroscopic measurements of IOM were conducted at the Earth and Planets Laboratory by Dionysis Foustoukos using a Jasco model NRS-3100 confocal Raman spectrometer. The Raman system is equipped with an excitation laser operating at 490.2 nm (λ_{ex} ; Coherent GENESIS MX-488). The output power measured on the samples ranged from 0.1 to 1 mW. Signal detection was accomplished through (i) an Olympus MPLN objective lens with a $100\times/0.90$ aperture leading to a beam diameter of ~ 1 μm , and (ii) an Olympus MPLN $20\times/0.45$ aperture with a beam diameter of ~ 4 μm . Spatial depth resolution is ~ 0.4 – 0.5 μm for the NRS-3100 confocal optics assuming an IOM refractive index that is similar to graphitic material. The acquisition time was dependent on the laser power and objective lens employed: (i) 240 s acquisition was applied at 0.1 mW and for the $20\times$ lens; (ii) 120 s at 0.1 mW and $100\times$; and (iii) 30 s for laser powers of 0.5–1 mW and for the $100\times$ lens. The adopted laser powers and acquisition times showed no evidence of laser-induced IOM degradation (see later in the Raman Results section), and they are in the same range as those employed in previous studies (Bonal et al., 2016; Busemann et al., 2007; Potiszil et al., 2021; Quirico

et al., 2018; Rotundi et al., 2008; Steele et al., 2018; Visser et al., 2018). Ten acquisitions per window were collected to allow for spectrum enhancement (Steele et al., 2018). The acquired spectral windows were centered at 1500 cm^{-1} with a frequency resolution of $<4\text{ cm}^{-1}$ at $1200\text{ grooves mm}^{-1}$. The signal was collected with a Peltier-cooled charge coupled device (CCD) at -69°C (Andor™ Model DV401-F1 1024×128 pixel with $25\text{ }\mu\text{m}$ pixel size). The system was equipped with a holographic notch filter. All the Raman spectra collected were unpolarized.

Raman vibrational spectra were collected from the IOM isolates of Murchison A and B, Sutter's Mill, PCA 91008, and WIS 91600 to characterize their molecular structures in connection to the crystalline and disordered carbonaceous materials identified by the vibrons (bands) at $\sim 1580\text{ cm}^{-1}$ (G; ω_G) and $\sim 1350\text{ cm}^{-1}$ (D; ω_D), respectively (Beysac et al., 2002; Pasteris & Chou, 1998). Curve-fitting and background subtraction of the Raman spectra were orchestrated using the commercial software Igor from Wavemetrics. In accordance with previous studies, peak fitting protocols resulted to lower residual by adopting Gaussian and/or Lorentzian distribution for the G band and Lorentzian for the D band (Foustoukos, 2012; Foustoukos et al., 2021). The integrated areas and FWHH of the Raman bands reflected the average values between Lorentzian and Gaussian fitting functions. Background subtraction was conducted by fitting third-order polynomials through portions of the spectra without signal intensity (Long, 1977). Measurements were conducted on individual grains using protocols that were developed to optimize acquisition conditions for the best signal to noise ratio. To this end, spectra were collected at a range of laser power ($0.1\text{--}1\text{ mW}$), for a range of acquisition times ($30\text{--}240\text{ s}$) and by adopting a $100\times$ or a $20\times$ objective lens. The lowest power distribution conditions on the sample surface were attained with the use of the $20\times$ lens ($4\text{ }\mu\text{m}$ beam size) at 0.1 mW , while the highest power distribution was established with the $100\times$ lens ($1\text{ }\mu\text{m}$ beam size) at 1.0 mW . Previous studies employed similar power density (Bonal et al., 2016; Busemann et al., 2007; Potiszil et al., 2021; Quirico et al., 2018; Rotundi et al., 2008; Steele et al., 2018; Visser et al., 2018).

XRF Spectroscopy of Bulk Meteorites

Bulk samples were subject to major and minor element analysis (Na, Mg, Al, Si, P, S, K, Ca, Ti, Cr, Mb, Fe, Co, Ni, Cu, Zn) were performed at the Earth and Planets Laboratory by Dionysis Foustoukos using a Spectro-XEPOS benchtop x-ray fluorescence energy-dispersive spectroscopy spectrometer equipped with a 50 Watt Pd end-window tube (50 kV max voltage) and a silicon drift detector (SDD) with spectral resolution of less than 160 eV for Mn K-alpha. The instrument employs

five secondary targets (Co, Pd, Mo, HOPG, Al_2O_3) to improve sensitivity for the analysis of elements from Na to U, and it operates under a helium atmosphere. Protocols have been developed to analyze powdered samples ($>0.1\text{ g}$) from a wide range of ultramafic, mafic, and felsic lithologies ($n = 72$; Guice et al., 2021). Accuracy is constantly monitored by analyzing international geochemical reference materials: GSJ JA-1, IGGE GSR-5, and IGGE GSD-12, with precision assessed by repeat analyses of the standards in different sample batches. Samples were analyzed in replicates. Loss of ignition was adjusted to account for the loss of H_2O and CO_2 volatiles as reflected by the H and C abundances of samples as determined by EA-IRMS.

Noble Gas Mass Spectrometry of Murchison (A and B) and Sutter's Mill IOM

Aliquots of IOM isolated from Murchison (A and B) and two aliquots of IOM from Sutter's Mill (see Table 5 for masses) were analyzed by Henner Busemann at ETH Zurich according to standard procedures as described previously in detail (Busemann et al., 2000; Riebe et al., 2017). Briefly, the samples were wrapped in 20 mg of Al foil and extracted in one step at nominally 1700°C in a Mo crucible heated by electron impact (EI). Full noble gas extraction was verified by a re-extraction step at slightly elevated temperature. Only the Ar, Kr, and Xe in Sutter's Mill IOM aliquot #1 (Table 5) were possibly not fully extracted in the main step ($2\text{--}3\%$ may have remained). The extracted gases were cleaned from reactive molecules, separated into He-Ne, Ar, and Kr-Xe-rich fractions, and analyzed for all stable noble gas isotopes. Blanks amount to $\leq 0.5\%$ of the measured intensities, respectively, for all isotopes except for ^{40}Ar , which is extremely low or absent in IOM and very abundant in air (Busemann et al., 2000).

RESULTS

Efficiency and Quality of IOM Isolation

The total time required to produce the IOM isolates was about 4 weeks. The IOM yields for Murchison A and B and Sutter's Mill were on a wt% basis 1.348% , 1.512% , and 1.854% , respectively. IOM yield typically accounts for approximately 50% or more of the bulk C contents of primitive chondrites (Alexander et al., 2017; Alexander & Pizzarello, 2015; Smith & Kaplan, 1970).

Elemental and Isotopic Analysis of Bulk and IOM Samples

Elemental and isotopic analyses for C, N, and H were performed on bulk Murchison A and B and Sutter's Mill

powders, as well as on IOM isolated from the respective meteorites. The bulk analyses of Murchison A and B (Table 1) are identical to one and another within the uncertainties of the measurements. However, the new analyses have a slightly lower C contents than previously reported for a different Murchison sample (Alexander et al., 2012). Compared to Murchison, the bulk Sutter's Mill sample exhibits lower elemental abundances and isotopic compositions for all three elements (Table 1). Included in Table 1 are previous bulk analyses of Sutter's Mill powder from the SM2, SM12, and SM51 stones (Jenniskens et al., 2012). It is clear from the data that Sutter's Mill bulk elemental and isotopic compositions vary significantly from sample to sample.

The elemental and isotopic compositions of Murchison A and B and Sutter's Mill IOM are shown in Table 2. The IOM extracted from Murchison A and B IOM is essentially identical within the measurement uncertainties; however, the C contents are slightly lower than has been reported before (Alexander et al., 2007). This results in slightly higher H/C atomic ratios (atom; Table 2) than what was measured on a previous Murchison IOM sample that was isolated from a different meteorite fragment. Elemental and isotopic H data have not been reported for Sutter's Mill IOM; to our knowledge, these are the first such values measured.

The levels of C and N contamination in the "witness plate" aluminum proxies were below detection limits (Table 1). These data indicate that the witness plates do not exhibit any significant or detectable contamination as could be determined via EA and IRMS.

¹H and ¹³C Solid-State NMR Spectroscopy of IOM

The ¹³C VACPMAS NMR spectra of Murchison A and B and Sutter's Mill IOM are presented in Figure 1. As has been observed previously, these ¹³C-NMR spectra consist of multiple overlapping peaks spanning the full range of chemical shifts for organic C (Cody et al., 2002;

Cody & Alexander, 2005; Gardinier et al., 2000). Clear separation of sp³ C (aliphatic) at low frequencies and sp² C (aromatic and carbonyl) at higher frequencies is observed. This separation arises from the fact that the electronic symmetry surrounding a ¹³C nucleus in sigma bonds is highly symmetrical, whereas with double bonds (π bonds), the electron density surrounding ¹³C is highly asymmetric. Rapid MAS serves to average chemical shielding anisotropy to a single average isotropic frequency, with the average sp² ¹³C at a significantly higher frequency than that of sp³ ¹³C. Another factor that controls the solid-state ¹³C-NMR frequency is the electronegativity of elements C is bonded to. In particular, C bonded directly to O is shifted to higher frequencies relative to C bonded to C or H. This is true for both sp³ and sp² C. This can be seen in the identity of the six spectral regions identified as distinct peaks and shoulders in the ¹³C-NMR spectra (Figure 1).

The ¹H solid-state NMR spectra of Murchison A and B and Sutter's Mill IOM are presented in Figure 2. Whereas ¹H only exists as sigma (single) bonds, ¹H bonded to doubled-bonded C (aromatic and/or olefinic H) is shifted to higher frequencies and for aliphatic H, ¹H peaks shift up slightly in frequency from CH₃ to CH₂ and CH; thus, the utility of ¹H solid-state NMR of IOM is predominantly to ascertain the proportions of aromatic H and aliphatic H, which provide a useful measure of the degree of IOM molecular evolution. For Murchison A and B IOM, three distinct spectral features are resolved with ¹H solid-state NMR at 22 kHz MAS, two associated with aliphatic-H and one associated with aromatic-H. For Sutter's Mill IOM, only two of these bands are clearly resolved (Figure 2).

From the spectra in Figure 1, the solid-state ¹³C-NMR spectra of Murchison A and B are indistinguishable, and the ¹³C-NMR spectrum of Sutter's Mill IOM contains a significant proportion of aromatic C (at ~130 ppm). Similarly, in the ¹H solid-state NMR spectra, Murchison A and B are indistinguishable, with

TABLE 1. Elemental and isotopic analyses of bulk samples.

Sample	H (wt%)	dD (‰)	C (wt%)	d ¹³ C ‰	N (wt%)	d ¹⁵ N ‰	H/C atom
Sutter's Mill	0.359 ± 0.018	-69.0 ± 1.5	1.65 ± 0.04	-8.7 ± 0.4	0.066 ± 0.002	18.1 ± 0.5	2.659 ± 0.15
Murchison A	1.058 ± 0.053	-33.2 ± 8.0	1.92 ± 0.02	-2.7 ± 0.4	0.101 ± 0.003	44.6 ± 0.2	6.613 ± 0.34
Murchison B	1.135 ± 0.057	-38.9 ± 3.8	1.98 ± 0.03	-2.5 ± 0.4	0.104 ± 0.003	45.8 ± 0.8	6.879 ± 0.35
Murchison prev. ^a	1.07 ± 0.002	-61.7 ± 3.1	2.08	-2.9	0.105	45.6	6.185
SM2 ^b	—	—	1.32 ± 0.03	-13 ± 1	0.0397 ± 7 ⁻³	16.7 ± 0.3	—
SM12 ^b	—	—	1.56 ± 0.01	2 ± 3	0.0404 ± 39 ⁻³	-0.02 ± 0.6	—
SM51 ^b	—	—	1.62 ± 0.01	-3 ± 1	0.0405 ± 4 ⁻³	6.2 ± 0.4	—
Witness plates	n/a	n/a	<0.01	n/a	<0.001	n/a	n/a

Note: Reported errors are at 1 s level and correspond to the highest values of variability observed in standards and replicates (*n* = 2).

^aAlexander et al. (2007).

^bJenniskens et al. (2012).

TABLE 2. Elemental and isotopic analyses of IOM.

Sample	H (wt%)	dD ‰	C (wt%)	d ¹³ C ‰	N (wt%)	d ¹⁵ N ‰	H/C atom	N/C atom
Murchison A	3.536 ± 0.177	796.7 ± 10.3	60.24 ± 1.49	-18.3 ± 0.2	2.44 ± 0.06	3.8 ± 0.2	0.70 ± 0.04	0.036 ± 0.001
Murchison B	3.434 ± 0.172	792.3 ± 5.1	59.58 ± 1.48	-18.6 ± 0.2	2.51 ± 0.06	4.9 ± 0.2	0.69 ± 0.04	0.035 ± 0.001
Sutter's Mill	2.004 ± 0.100	28.4 ± 8.1	66.21 ± 1.64	-13.8 ± 0.2	2.46 ± 0.06	21.5 ± 0.2	0.36 ± 0.02	0.032 ± 0.001
SM12 and SM41 ^a	—	—	39	-26	1.9	2.5	—	—
Murchison prev. ^b	3.254 ± 0.082	777 ± 27	66.5 ± 0.6	-18.91 ± 0.01	2.54 ± 0.05	-1.0 ± 0.04	0.58 ± 0.02	0.033 ± 0.001

Note: Reported errors are at 1 s level and correspond to the highest values of variability observed in standards and replicates (for H analyses $n = 2$, for C-N analyses $n = 1$).

^aCombined IOM from two different SM (12 and 41) stones, Pizzarello et al. (2013).

^bAlexander et al. (2007).

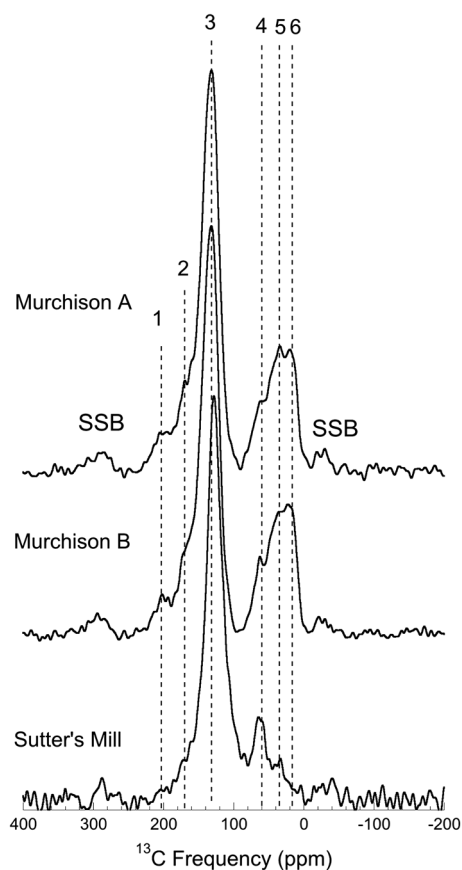


FIGURE 1. ^{13}C solid-state NMR spectra of IOM isolated from Murchison A and B and Sutter's Mill carbonaceous chondrites. Peak 1 corresponds to ketone carbonyl; peak 2 corresponds to carboxyl C; peak 3 corresponds to aromatic and olefinic C; peak 4 corresponds to alcohol or ether; peak 5 corresponds to methylene and methine (CH_2 and CH); peak 6 corresponds to methyl C (CH_3). The peaks labeled SSB are spinning sidebands arising from incomplete MAS averaging of the aromatic chemical shielding anisotropy.

obvious subordinate aromatic-H peaks at ~ 7 ppm, and two peaks in the aliphatic-H region at ~ 3.2 and 1.5 ppm that correspond to $\text{CH}_2 + \text{CH}$ and CH_3 , respectively (Pretsch et al., 2000). The Sutter's Mill IOM ^1H -NMR spectrum differs considerably from Murchison A and B, revealing only aromatic-H and $\text{CH}_2 + \text{CH}$ intensity (CH_3 intensity is absent or very weak), where the aromatic H intensity is clearly dominant over the aliphatic H intensity.

For quantitative comparison, both the ^{13}C and ^1H solid-state NMR spectra are integrated to obtain representative peak areas corresponding to the various spectral regions (Table 3) as shown in Figures 1 and 2. Given the extensive peak overlap observed in both the ^{13}C and ^1H solid-state spectra, there is only one proper way to do this. Fortunately, the ^1H and ^{13}C -NMR isotropic frequency ranges for each of the major functional groups

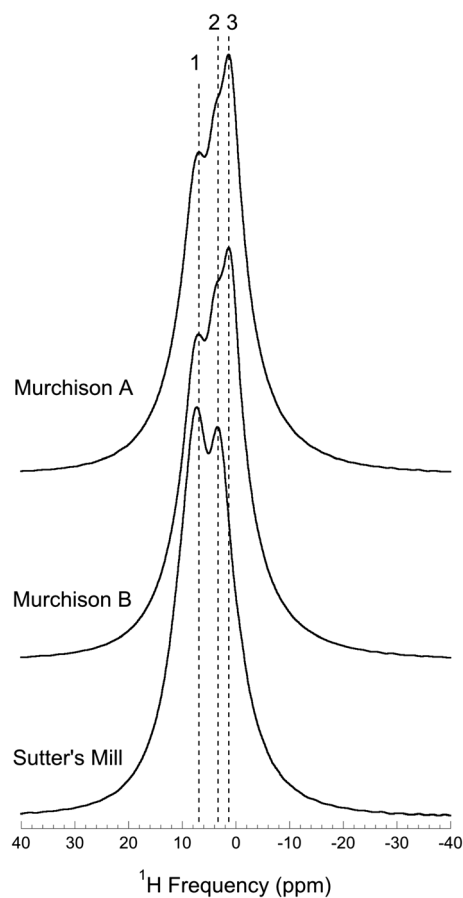


FIGURE 2. ^1H solid-state NMR spectra of IOM isolated from Murchison A and B and Sutter's Mill carbonaceous chondrites. Peak 1 corresponds to aromatic/olefinic H; peak 2 corresponds to methylene and methine (CH_2 and CH) H; peak 3 corresponds to methyl H (CH_3).

in IOM are well determined (Pretsch et al., 2000). For quantitation, we integrate the NMR signal across discrete frequency domains. The sp^3 ^{13}C region (including CH_3 , CH_2 , CH , and $\text{CH}_x\text{-O}$ carbon) is clearly defined as ranging from 0 to 90 ppm, the aromatic C region (including aromatic, olefinic and enolic $\text{C}=\text{C}$) ranges from 90 to 160 ppm, and the carbonyl (including ketone, quinone, aldehyde and carboxylic $\text{C}=\text{O}$) ranges from 160 to 230 ppm. The intensity of the spinning sidebands (that result from incomplete MAS averaging of $\text{C}=\text{C}$ chemical shielding anisotropy) span the frequency ranges of -60 to 0 ppm, and 280 to 340 ppm; the peak areas must be added to the aromatic C intensity to properly determine the fraction of aromatic C ($F_{\text{Aro-C}}$).

For the ^1H solid-state NMR, we identify the break between aromatic H and aliphatic H at 5.1 ppm. Thus, the intensity ranging from -40 to 5.1 ppm corresponds to aliphatic H and the range from 5.1 to 40 ppm corresponds to aromatic H. Using such intensity ranges

TABLE 3. ^1H and ^{13}C solid-state NMR functional group concentration determination.

Functional group	Murchison A	Murchison B	Sutter's Mill
Spinning sideband low freq., ^{13}C -NMR ^a	0.03	0.02	0.03
Aliphatic CH_x , ^{13}C -NMR ^b	0.28	0.29	0.19
Aromatic and olefinic $\text{C}=\text{C}$, ^{13}C -NMR	0.50	0.52	0.67
Carbonyl, ^{13}C -NMR ^c	0.14	0.13	0.07
Spinning sideband high freq., ^{13}C -NMR ^a	0.04	0.03	0.03
Fraction aromatic C, ^{13}C -NMR ^d	0.58 ± 0.01	0.58 ± 0.01	0.74 ± 0.02
Aliphatic H ^1H -NMR	0.60	0.60	0.47
Aromatic H ^1H -NMR	0.40	0.40	0.53

^aSpinning sidebands represent residual intensity due to chemical shielding anisotropy largely from $\text{C}=\text{C}$, these reside at $\pm\text{MAS}$ frequency off the main aromatic band at ~ 130 ppm.

^b CH_x includes CH_3 , CH_2 , CH and alcohols and/or ethers.

^cCarbonyl ($\text{C}=\text{O}$) includes carboxylic groups, quinones, and ketones/aldehydes.

^dFraction of aromatic carbon (FA) includes aromatic/olefinic "C" plus spinning sideband intensities.

for ^1H and ^{13}C -NMR spectra avoids the need to guess about the peak shapes that are typically variable mixes of Lorentzian and Gaussian line shapes and cannot be constrained with so much peak overlap. The precision of the integrated areas is a function of the ratio of signal of the peaks relative to the baseline noise, or SNR. The SNR of the ^1H -NMR spectra is very large (due to the high natural abundance of ^1H and its large magnetic moment), and the precision uncertainty is vanishingly small.

For the much less sensitive ^{13}C (with low natural isotopic abundance and a magnetic moment 25% that of ^1H), key parameters such as the fraction of aromatic C, $F_{\text{Aro-C}}$, have a precision of ± 0.01 (based on the SNR) for Murchison A and B NMR data. As evident in Figure 1, the SNR of the Sutter's Mill IOM ^{13}C solid-state NMR spectrum is slightly poorer and the uncertainty in determining $F_{\text{Aro-C}}$ is ± 0.02 (Figure 1). The quantified ^1H and ^{13}C -NMR data for all three IOM samples are presented in Table 3, supporting the similarities and dissimilarities in molecular structure of these three IOM samples that are evident in Figures 1 and 2.

Raman Spectroscopy of IOM

Results indicate that laser-induced heating, at the conditions employed, did not alter the IOM structure. This was demonstrated in the low-fluorescence spectra collected from individual WIS 91600 IOM grains across the entire range of power distributions investigated (Figure 3a). For the purpose of assessing whether XCT analysis perturbed the Raman spectra of Murchison IOM we focused on the vibrational characteristics of the G and D bands (Busemann et al., 2007; Quirico et al., 2014, 2018). The observed frequencies of ω_{G} for Murchison A and B are 1583 and 1581 cm^{-1} , respectively; the ω_{D} for Murchison A and B is 1362 ± 9 cm^{-1} and 1360 ± 8 cm^{-1} , respectively (Figure 3b). The attained full width at half height (Γ , cm^{-1}) for the G band in Murchison A & B are Γ_{G} are 97 ± 4 cm^{-1} and 99 ± 6 cm^{-1} , respectively; the Γ_{D} for Murchison A & B is 308 ± 22 cm^{-1} and 301 ± 17 cm^{-1} , respectively. These values are close to what others have measured for Murchison IOM (Busemann et al., 2007; Foustoukos, 2012; Quirico et al., 2014, 2018). It is concluded that XCT does not change the Raman spectra of IOM. The observed frequency of ω_{G} for Sutter's Mill IOM is 1584 cm^{-1} (with $\Gamma_{\text{G}} = 93 \pm 10$ cm^{-1}) and the ω_{D} for is 1361 ± 6 cm^{-1} (with $\Gamma_{\text{D}} = 275 \pm 9$ cm^{-1}) which are in close agreement with what has previously been reported (Quirico et al., 2018). In the WIS 91600 IOM, we observed nearly identical vibrational characteristics with the Sutter's Mill, while in the PCA 91008, the Γ_{D} was slightly narrower (258 ± 10 cm^{-1}). This is consistent with previous Raman analysis of Sutter's Mill and PCA 91008 organic residues (Beck et al., 2014).

Overall, the Raman spectra collected are in good agreement with previous spectroscopic studies on Murchison, Sutter's Mill, PCA 91008, and WIS 91600 (Beck et al., 2014; Busemann et al., 2007; Foustoukos et al., 2021; Quirico et al., 2018; Starkey et al., 2013). Interestingly, the Murchison samples are significantly more fluorescent than the Sutter's Mills, PCA 91008 and WIS 91600 IOM residues (Figure 3a,b), while attaining broader Γ_{D} and Γ_{G} values (Figure 3c). Low fluorescence in IOM samples is generally associated with higher degrees of thermal metamorphism in chondrites (Bonal et al., 2016) and with an elevated concentration of aromatic moieties in coals (Munoz Caro et al., 2006; Zhu et al., 2023). Similarly, the wider Γ_{D} observed in Murchison A and B relative to the other IOM residues suggests lower degree of graphitic C crystallinity, probably associated with conditions of a lower thermal regime (Busemann et al., 2007; Cody et al., 2008; Homma et al., 2015; Pasteris & Wopenka, 1991; Wopenka & Pasteris, 1993). These observations are consistent with the positive correlation identified between Raman spectra and

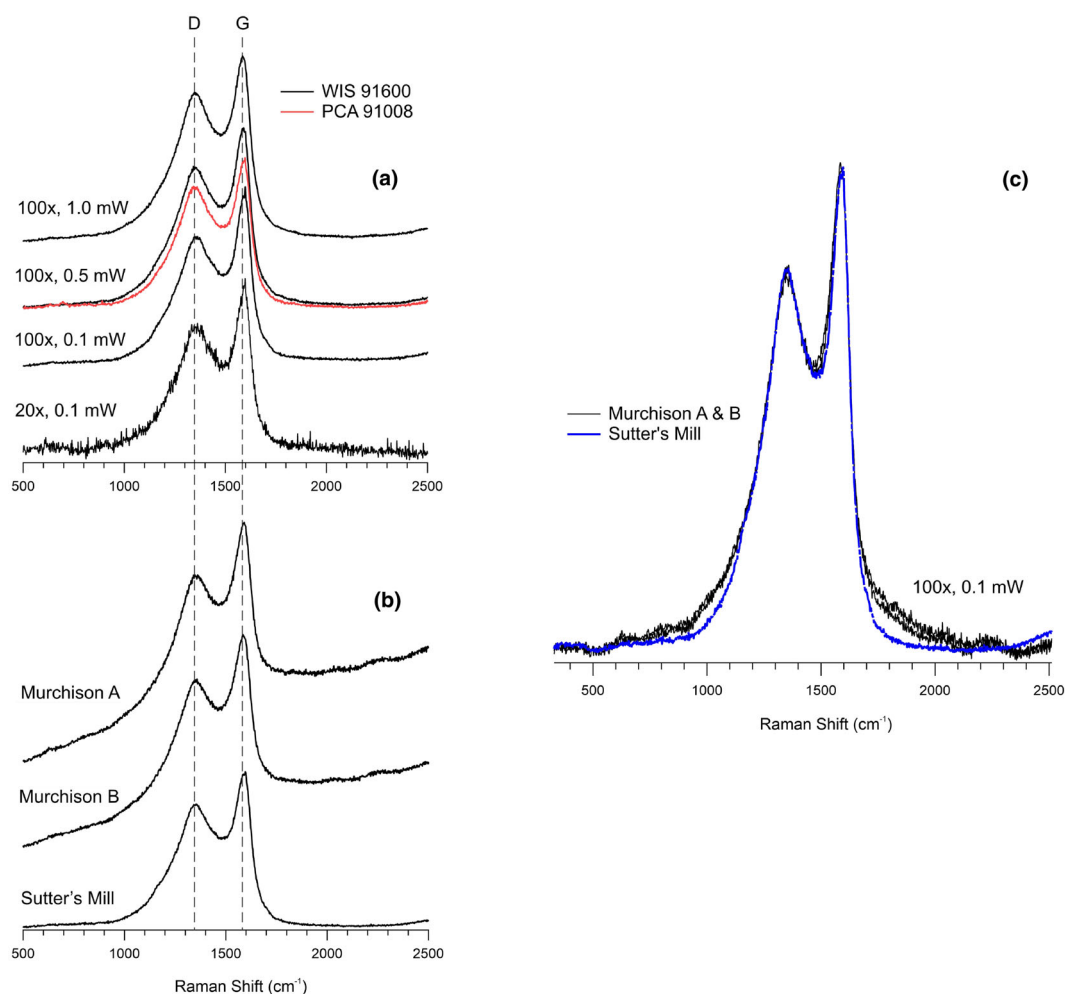


FIGURE 3. Raman vibrational spectra of IOM from WIS 91600 performed at a range of power distribution levels; PCA 91008, Murchison A and B, and Sutter's Mill conducted by using a 100 \times objective lens at 0.5 mW. (a) Results show that over the range of laser powers, the Raman spectra of the organic residues do not change. (b, c) Data revealed no significant differences between the Raman features of Murchison A and B arising from XCT. The Raman spectrum of Sutter's Mill (SM1 and SM8 combined) exhibits considerably lower fluorescence background than that observed for the Murchison organic residues, while registering narrower widths for the ω_G and ω_D bands (c). Dotted lines trace the D and G vibrational bands attributed to the ordered and disordered structure of carbonaceous material. In (c), the spectra shown are those from (b) after background subtraction. (Color figure can be viewed at [wileyonlinelibrary.com](https://onlinelibrary.wiley.com/doi/10.1111/maps.14096))

degree of aromaticity ($F_{\text{Aro-C}}$; Table 3) for the IOM samples studied here.

XRF Spectroscopic Analysis of Bulk Meteorite Samples

The major and minor element XRF analysis of the Murchison A and B and Sutter's Mill bulk samples was conducted on aliquots with sample sizes ranging from 79 to 102 mg and with a maximum particle size less than 100 μm (Glavin et al., in review). The elemental compositions of the Murchison A and B are nearly identical with small deviations from previous analyses (Table 4). In detail, the new samples appear to be depleted in Na, Al, K, and Fe, and less so in Co, Ni, and Zn

compared to the values that were previously measured by XRF, inductively coupled plasma mass spectrometry (ICP-MS) and instrumental neutron activation analysis (INAA; Braukmüller et al., 2018; Kallemeyn & Wasson, 1981; Wolf & Palme, 2001). Thus, the elemental depletions observed might be associated with analytical challenges induced by sample size limitations (<0.1 g). Overall, the attained XRF chemical compositions of Murchison A and B, and Sutter's Mill are consistent with the expected composition of CM chondrites (Alexander, 2019). This demonstrates the efficiency of our XRF analytical protocols to measure major and minor elemental compositions of bulk chondritic samples with sample sizes of nearly 0.1 g.

TABLE 4. X-ray fluorescence analyses of bulk samples.

	Murchison A	Murchison B	Sutter's Mill	CM ^a	MUR ^b	MUR ^c	MUR ^d	SM ^e
Sample size (mg)	79.1	102	85.05					
Na (mg g ⁻¹)	b.d.	0.25 ± 0.35	1.20 ± 0.38	4.15	0.875	4.27		4.7–5.7
Mg (mg g ⁻¹)	122	115	120	117	121–123	126	121	127–137
Al (mg g ⁻¹)	7.44	7.66	8.69	11.6	11.4–12.1	12.7	11.6	12.7–13.4
Si (mg g ⁻¹)	141	130	138	130			134.8	135–137
P (mg g ⁻¹)	1.15	1.08	1.28	0.98	1.0–1.1		1.06	1.1–1.3
S (mg g ⁻¹)	21.6	20.7	25.3	33	24.5–26.3			27.7–31.4
K (μg g ⁻¹)	381 ± 40	353	315 ± 74	403	496–1411	404		363
Ca (mg g ⁻¹)	12.8	13.0	15.9	12.4	11.5–11.8	14.5	12.5	14.1–21.1
Ti (μg g ⁻¹)	626	641	751	619	564–579		650	560–700
Cr (mg g ⁻¹)	2.61	2.67	3.05	3.06	3.2–3.3	3.09	3.07	3.1–3.4
Mn (mg g ⁻¹)	1.38	1.48	1.76	1.71	1.76–1.86	1.76	1.72	1.7–1.9
Fe (mg g ⁻¹)	156	175	200	212	219–226	209	214	222–228
Co (μg g ⁻¹)	463	521	605	579	600–612	586		450–585
Ni (mg g ⁻¹)	7.69	8.84	10.5	12.1		11.8		10
Cu (μg g ⁻¹)	89	103	133	123	136–142			135–200
Zn (μg g ⁻¹)	126	152	171	180	192–201	189		187–250

Note: Replicate analyses with 1 s errors at <5%, except when specified otherwise.

Abbreviation: b.d., below detection.

^aAlexander (2019).

^bBraukmüller et al. (2018).

^cKallemeyn and Wasson (1981).

^dWolf and Palme (2001).

^eJenniskens et al. (2012).

Noble Gas Analysis of the IOM

Data for the four IOM residue samples are given in Table 5. Noble gases in IOM are carried by embedded refractory presolar grains such as nano-diamonds, SiC, and graphite (mainly but not exclusively He and Ne (e.g., Ott, 2014; Zinner, 2014) and an elusive, possibly macromolecular C-rich material dubbed “phase Q” (small amounts of He and Ne but most of the IOM's Ar, Kr, and Xe; Busemann et al., 2000; Lewis et al., 1975). X-ray-induced effects might be detectable in (i) lower concentrations in Murchison IOM B relative to A and (ii) a possible shift in isotope and element ratios if the mixing ratio of presolar grains to phase Q is affected. However, sample heterogeneity at the ~1 mg sample scale must be considered first.

A measure for heterogeneity is given by the two Sutter's Mill IOM aliquots taken from the same IOM powder (Table 5). Concentrations of the reference isotopes of each element vary only within their uncertainties of typically 1%–3%, and element ratios are thus also strikingly similar, illustrating that heterogeneity is no reason for concern measuring gas concentrations in IOM aliquots at the ~1 mg mass level. Similarly, almost all isotope ratios measured in the Sutter's Mill IOM aliquots #1 and #2 agree within uncertainty. Deviations between these aliquots exceeding the uncertainties are only visible in ²¹Ne/²²Ne,

^{124,126,134}Xe/¹³²Xe, possibly caused by slightly distinct contributions of cosmogenic ²¹Ne (from refractory minerals embedded in the IOM) and air Xe.

The level of variations in Murchison IOM is very similar to that in Sutter's Mill IOM. Beyond uncertainty, there is no deviation in B relative to A apart from the ⁴He concentration, which is 2.7% lower in Murchison B, but still in the expected range in view of the Sutter's Mill IOM variations. All isotope ratios apart from ^{129,134,136}Xe/¹³²Xe are, within uncertainties, identical.

There is a small depletion (5%–3%) of the lighter elements (He, Ne, Kr) normalized to the heavier Xe in Murchison B relative to Murchison A, producing a mass-dependent trend. At first view, this could be taken as evidence for the loss of the lighter, more diffusive elements relative to Xe due to XCT-induced alteration. However, a slightly decreased concentration of presolar grains (carrying mainly He, Ne) relative to phase Q (Xe) in Murchison B compared to Murchison A could equally explain this trend. This trend in the element ratios is marginal compared to other observed variations and almost completely covered by the uncertainties.

Murchison and Sutter's Mill IOM data from this study compare well with literature data (Busemann et al., 2000, 2008; Spring et al., 2011; Srinivasan, 1977; Wieler et al., 1992). Gas concentrations monitor conditions experienced on the parent bodies (thermal and aqueous alteration, e.g., Busemann et al., 2000). These cause

TABLE 5. Noble gases in Murchison and Sutter's Mill IOM. Concentrations of ^4He , ^{20}Ne , and ^{36}Ar in $10^{-8}\text{ cm}^3\text{ STP g}^{-1}$; ^{84}Kr and ^{132}Xe in $10^{-10}\text{ cm}^3\text{ STP g}^{-1}$. All Kr and Xe isotope ratios given $\times 100$.

	Mass (mg)	^4He	$^3\text{He}/^4\text{He} \times 10^4$	^{20}Ne	$^{20}\text{Ne}/^{22}\text{Ne}$	$^{21}\text{Ne}/^{22}\text{Ne}$		
Murchison IOM A (MurA)	1.799 \pm 0.015	196,400 \pm 1800	1.703 \pm 0.025	642.2 \pm 6.0	7.749 \pm 0.027	0.02813 \pm 0.00025		
Murchison IOM B (MurB)	1.397 \pm 0.017	191,200 \pm 2400	1.695 \pm 0.034	631.5 \pm 8.8	7.714 \pm 0.039	0.02786 \pm 0.00034		
Sutter's Mill IOM (SM#1)	0.824 \pm 0.016	144,800 \pm 2900	1.481 \pm 0.046	495.1 \pm 10.0	7.871 \pm 0.034	0.02757 \pm 0.00024		
Sutter's Mill IOM (SM#2)	1.240 \pm 0.014	144,000 \pm 1700	1.486 \pm 0.027	495.0 \pm 6.0	7.875 \pm 0.031	0.02834 \pm 0.00021		
	^{36}Ar	$^{36}\text{Ar}/^{38}\text{Ar}$	$^{40}\text{Ar}/^{36}\text{Ar}$	^{84}Kr	$^{78}\text{Kr}/^{84}\text{Kr}$	$^{80}\text{Kr}/^{84}\text{Kr}$	$^{82}\text{Kr}/^{84}\text{Kr}$	$^{83}\text{Kr}/^{84}\text{Kr}$
MurA	3360 \pm 110	5.302 \pm 0.014	0.357 \pm 0.012	37.04 \pm 0.47	0.5888 \pm 0.0049	3.849 \pm 0.028	19.87 \pm 0.15	19.91 \pm 0.11
MurB	3410 \pm 110	5.306 \pm 0.021	0.3215 \pm 0.0100	37.49 \pm 0.56	0.5931 \pm 0.0058	3.844 \pm 0.025	19.83 \pm 0.12	19.86 \pm 0.11
SM#1	2398 \pm 50	5.321 \pm 0.021	0.667 \pm 0.070	28.86 \pm 0.61	0.5982 \pm 0.0059	3.891 \pm 0.029	19.95 \pm 0.12	19.913 \pm 0.093
SM#2	2374 \pm 31	5.297 \pm 0.015	0.581 \pm 0.049	28.37 \pm 0.40	0.5970 \pm 0.0067	3.864 \pm 0.022	20.17 \pm 0.11	19.921 \pm 0.091
	$^{86}\text{Kr}/^{84}\text{Kr}$	^{132}Xe	$^{124}\text{Xe}/^{132}\text{Xe}$	$^{126}\text{Xe}/^{132}\text{Xe}$	$^{128}\text{Xe}/^{132}\text{Xe}$	$^{129}\text{Xe}/^{132}\text{Xe}$	$^{130}\text{Xe}/^{132}\text{Xe}$	
MurA	19.91 \pm 0.11	45.69 \pm 0.62	0.4673 \pm 0.0037	0.4073 \pm 0.0029	8.110 \pm 0.046	104.52 \pm 0.63	15.961 \pm 0.096	
MurB	19.86 \pm 0.11	0.4670 \pm 0.0050	0.4086 \pm 0.0023	8.048 \pm 0.037	103.07 \pm 0.58	15.880 \pm 0.077	46.90 \pm 0.74	
SM#1	19.913 \pm 0.093	39.49 \pm 0.86	0.4572 \pm 0.0041	0.4055 \pm 0.0033	8.120 \pm 0.037	103.75 \pm 0.50	16.064 \pm 0.087	
SM#2	19.921 \pm 0.091	39.16 \pm 0.58	0.4470 \pm 0.0041	0.3972 \pm 0.0031	8.084 \pm 0.037	103.18 \pm 0.42	15.983 \pm 0.059	
		$^{131}\text{Xe}/^{132}\text{Xe}$		$^{134}\text{Xe}/^{132}\text{Xe}$		$^{136}\text{Xe}/^{132}\text{Xe}$		
MurA		82.19 \pm 0.48		38.27 \pm 0.28		32.19 \pm 0.19		
MurB		82.10 \pm 0.34		37.64 \pm 0.16		31.60 \pm 0.14		
SM#1		82.37 \pm 0.43		38.34 \pm 0.23		32.07 \pm 0.21		
SM#2		81.63 \pm 0.29		37.83 \pm 0.13		32.24 \pm 0.13		

variations in concentrations ranging over two (Kr, Xe) to three (He, Ne) orders of magnitude. Even within the same study (IOM in Murchison, produced according to the "Chicago recipe" with HF/HCl, Wieler et al., 1992), gas concentrations can scatter with factors of a few percent.

DISCUSSION

The aim of this study was threefold: First, to prepare for analysis of the Bennu samples returned by OSIRIS-REx, our effort is intended to provide a demonstration of critical capabilities to fulfill specific analytical roles in the analysis of bulk material and IOM in Bennu samples, as well as a refinement of the time required to achieve the stated mission objectives. Second, by studying two samples of Murchison, one subjected to XCT (B) and the other a non-irradiated control (A), to look for evidence of organic matter transformation due to sample irradiation with high-energy x-rays. Third, to extract useful cosmochemical information from the measurements of Sutter's Mill IOM in context with that isolated from other CMs (Cody et al., 2002; Cody & Alexander, 2005). We discuss the latter two aims in this section.

Effects of XCT Analysis on IOM Molecular Structure and Composition

X-ray irradiation has the potential for destruction or modification of organic matter. The x-ray source energy

in this study was 160 keV, but below this maximum energy, there is a nearly continuous spectrum of x-rays generated through Bremsstrahlung emission. Damage of organic matter during irradiation is not from the photons directly, but rather because the passage of x-rays through matter generates free electrons with a wide range of kinetic energies (e.g., Auger and other secondary electrons), some of which may have sufficient kinetic energy to break covalent bonds (these can be generated both by resonant core-level electron ionization and by Compton scattering at higher energies). Much in the same way that aromatic molecules (with carbon double bonds) tend to remain largely intact during EI ionization in the source of a typical mass spectrometer, aliphatic molecules (with carbon single bonds) tend to fragment extensively, the same will be expected from organic matter being in proximity to x-ray-generated secondary electrons with sufficient kinetic energy (Cody et al., 2009).

The expected signature of x-ray-induced secondary electron damage of IOM in bulk Murchison powder would be a significant loss of aliphatic C moieties (increasing the fraction of aromatic C and H) and a corresponding reduction in the total H/C. In the present study, no differences in molecular structure of IOM from Murchison A and B are observed, that is, in level of aromaticity, H/C (Figure 1, Tables 2 and 3), Raman vibrational spectra (Figure 3), aliphatic and aromatic ^{13}C abundances (^{13}C solid-state NMR, Figure 1 and Table 3), and aliphatic and aromatic H abundances (^1H solid-state

NMR, Figure 2, Table 3). Similarly, there were no observable effects on the H-C-N elemental and isotopic composition of organic residues (Table 2). In view of the typically large variations in noble gas concentrations and compositions in IOM, created by (a) parent body processing and (b) possibly slightly heterogeneous distributions of presolar grains in IOM at the milligram level, the small observed variations between Murchison IOM A and B observed here at the low percent level are negligible and well explained by natural processes prior to examination with XCT.

Therefore, at the level of detection afforded by all the methods employed here, we conclude that x-ray irradiation during XCT imparted no detectable x-ray beam-derived secondary electron damage to chondritic IOM.

Comparison of the New Murchison IOM and the Sutter's Mill IOM with Other CMs

IOM from a variety of type 1 and 2 carbonaceous chondrites demonstrates a wide range of molecular structures that have been interpreted to represent varying degrees of molecular evolution due to parent body processing (e.g., hydrothermal alteration; Cody & Alexander, 2005). A study of the Tagish Lake meteorite revealed that considerable variation in IOM molecular structure can exist in various clasts from a single meteoroid (Alexander et al., 2014; Herd et al., 2011). Differences in IOM elemental chemistry (e.g., H/C, N/C) and molecular characteristics (e.g., fraction of aromatic C and aromatic H) in Tagish Lake clasts are indicative of differing extents of irreversible molecular evolution, where the direction of such transformation is toward lower H/C and N/C and larger $F_{\text{Aro-C}}$. In anticipation of the return of Bennu material, therefore, it is important to identify the range of IOM compositions we could encounter and to understand the processes that produced them. The H/C atomic ratios and $F_{\text{Aro-C}}$ of IOM isolated from the Tagish Lake clasts (Alexander et al., 2014; Herd et al., 2011) exhibit an extensive molecular evolution, where clast 5b is the most pristine and TL "orig" is the most evolved (Figure 4).

In this study, it is striking that Murchison samples A and B have larger H/C values than a previously analyzed sample of Murchison IOM (Table 2). Similarly, Murchison A and B have smaller $F_{\text{Aro-C}}$ values than that of the earlier Murchison IOM sample (Table 3). The earlier Murchison IOM had a H/C $\times 100$ and $F_{\text{Aro-C}}$ nearly identical to that of Tagish Lake 11 h, whereas the new Murchison A and B IOM plot midway between TL clasts 5b and 11 h (Figure 4).

The composition of Sutter's Mill's IOM suggests considerable molecular evolution (Figure 4, Tables 2 and

3), with H/C and $F_{\text{Aro-C}}$ lying between Tagish Lake clast 11v and "orig." The fact that CM IOM can span nearly the same range of molecular evolution as exhibited in the IOM from the Tagish Lake clasts suggests that such variation might not be rare. But, as ^{13}C solid-state NMR and elemental/isotopic analyses of IOM are very rarely done on multiple fragments of a given meteorite (e.g., Murchison), such variations in molecular evolution might largely go unnoticed. Variations in the molecular evolution of Sutter's Mill IOM in different stones (e.g., SM12 and SM2) were reported based on Raman spectroscopy (Beck et al., 2014; Jenniskens et al., 2012), but have yet to be systematically followed up with elemental, isotopic, and NMR analyses.

IOM from individual Tagish Lake clasts demonstrates a highly systematic change (depletion) in δD with molecular evolution (Alexander et al., 2014; Herd et al., 2011), as is shown in Figure 5. Interestingly, in a study where Murchison IOM was hydrothermally altered at temperatures ranging from 270 to 330°C for 72 h in sealed vessels, a similar trend of δD versus H/C emerged with a nearly identical slope to that of the Tagish Lake trend but with a consistent offset in δD of $\sim 500\%$ (Oba & Naraoka, 2009). Also plotted in Figure 5 are the

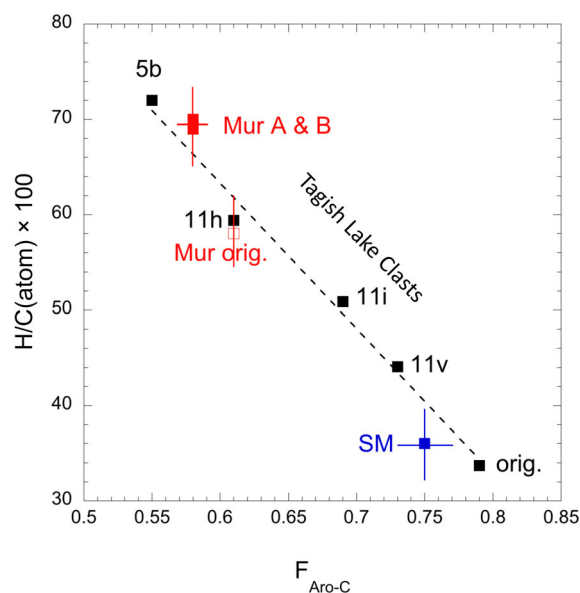


FIGURE 4. H/C (atom) $\times 100$ plotted against the fraction of aromatic carbon C ($F_{\text{Aro-C}}$) derived from ^{13}C solid-state NMR. In black are previous values for the various Tagish Lake clasts (Alexander et al., 2014; Herd et al., 2011); Murchison A and B are presented as solid red squares. A previous analysis of another sample of Murchison (Alexander et al., 2007; Cody et al., 2002; Cody & Alexander, 2005) is plotted as an open red square. Sutter's Mill IOM is presented as a solid blue square. The direction of IOM molecular evolution is from high to low H/C $\times 100$ and low to high $F_{\text{Aro-C}}$. (Color figure can be viewed at wileyonlinelibrary.com)

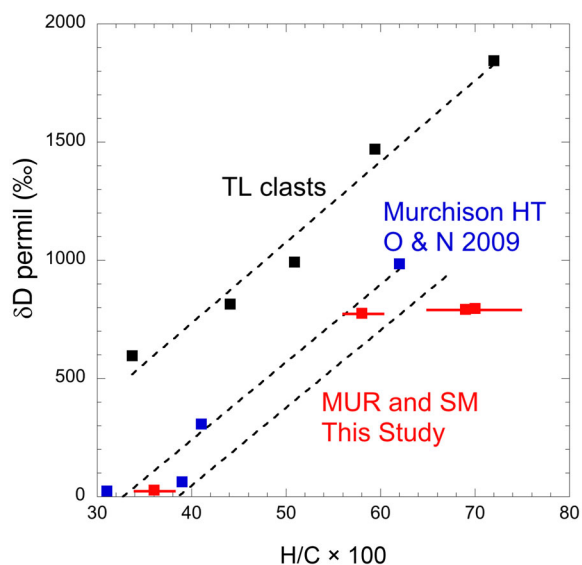


FIGURE 5. δD in permil (‰) plotted against $H/C(\text{atom}) \times 100$ for IOM derived from Tagish Lake clasts (Herd et al., 2011) with solid black squares, Murchison IOM hydrothermally heated at 270, 300, and 330°C for 72 h (Oba & Naraoka, 2009) with solid blue squares, and Murchison A and B from this study and previous Murchison analysis (Cody et al., 2002; Cody & Alexander, 2005) with solid red squares. In all three cases, the general trend is that with increased molecular evolution (decreasing $H/C(\text{atom}) \times 100$), the bulk δD drops significantly. (Color figure can be viewed at wileyonlinelibrary.com)

corresponding δD and H/C values for Murchison A and B (Table 2), the previously analyzed Murchison IOM sample (Alexander et al., 2007), and Sutter's Mill IOM (Table 2). A line with identical slope to the Tagish Lake trend is imposed on these data, potentially supporting the possibility that a Tagish Lake-like trend also exists with IOM from different CM clasts. In summary, Sutter's Mill IOM bears elemental, isotopic, spectroscopic (Raman), and molecular signatures of having experienced considerable molecular evolution akin to the most evolved Tagish Lake sample (Alexander et al., 2014; Cody & Alexander, 2005). A similar conclusion was drawn from Raman spectroscopy (Quirico et al., 2018).

The Molecular Structure of Sutter's Mill IOM in Relation to that of Other Heated CMs

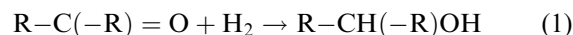
The so-called "heated" CMs are meteorites that have been interpreted to have experienced thermal metamorphism that was more intense than typical for CMs (Nakamura, 2005). We isolated IOM from two such heated CM meteorites: PCA 91008 and Wisconsin Range WIS 91600 in previous studies. ^{13}C solid-state NMR of both of these heated CMs has been published previously (Yabuta et al., 2010) and is reproduced here. ^1H solid-state NMR of IOM from these two meteorites had not been

obtained previously, so ^1H -NMR spectra were acquired in the present study, as these data provide insight into and allow for comparison across IOM molecular structures.

The ^{13}C solid-state NMR spectra of Sutter's Mill IOM are compared to WIS 91600, Tagish Lake "orig," and PCA 91008 in Figure 6. The ^{13}C -NMR spectra of all four meteorites share the common features of a strong predominance of aromatic C (large $F_{\text{Aro-C}}$; peak 4) and low H/C atomic ratios (Table 2 and Yabuta et al., 2010). Thus, all four IOM molecular structures carry signatures of considerable molecular evolution (Figure 4). Notwithstanding their similarly large values of $F_{\text{Aro-C}}$, the remaining C functionality varies considerably among these four IOM samples. For example, IOM from PCA 91008 and Tagish Lake "orig" have relatively high abundances of carbonyl C (peaks 1, 2, and 3, Figure 5), whereas WIS 91600 exhibits less carbonyl C and Sutter's Mill has the least carbonyl C (Figure 5).

One of the more striking differences observed in Figure 6 is the relative abundance of CH_xO groups (that are alcohols or ethers) at 65 ppm. This functional group is very prominent in Sutter's Mill's IOM and to a lesser extent in WIS 91600, Tagish Lake "orig," and PCA 91008 IOM. There is also variation among the samples in the relative concentrations of methylene (CH_2 , at 18 ppm) and methyl (CH_3 at 6 ppm) groups, where the former is present in all four IOM samples, but the latter is present only in Tagish Lake "orig" and PCA 91008. It is clear that whereas the predominant effect of molecular evolution is to increase $F_{\text{Aro-C}}$, at a more subtle level, other molecular outcomes are possible.

The presence of significant CH_xO intensity and depleted carbonyl C in Sutter's Mill IOM (Figures 2 and 6) relative to other highly molecularly evolved IOM samples is particularly intriguing. Under certain circumstances, carbonyl (in both ketone and carboxylic acid groups) can be reduced to an alcohol, for example, Equation (1) where a ketone is reduced to a secondary alcohol:



However, without the presence of a catalyst, molecular H_2 is unlikely to reduce a carbonyl to an alcohol (March, 1992).

Fortunately, other molecules that are hydride donors are well suited for such a reduction. Sodium borohydride (NaBH_4) and lithium aluminum hydride (LiAlH_4) are two common reducing agents used in organic chemistry (March, 1992). To test whether the carbonyls in IOM-like organic solids could be reduced to alcohol, analog IOM residues (syn-IOM) were reacted with NaBH_4 (see Methods). The starting syn-IOM and the reduced product were characterized using ^{13}C solid-state NMR

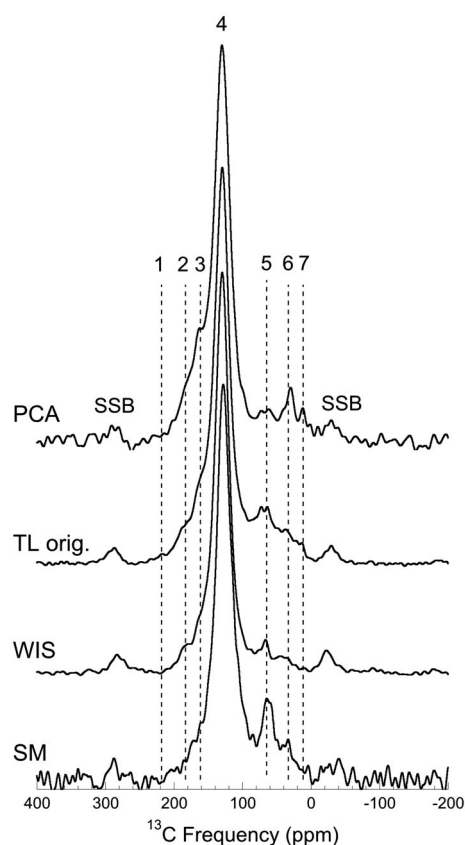


FIGURE 6. ^{13}C solid-state NMR of IOM isolated from Sutter's Mill, WIS 91600 (Yabuta et al., 2010), Tagish Lake "orig." (Cody & Alexander, 2005), and PCA 91008 (Yabuta et al., 2010). Peak 1 corresponds to where aliphatic ketone carbon C is expected; peak 2 corresponds to carboxyl carbon; peak 3 corresponds to "ene" carboxyl carbon; peak 4 corresponds to aromatic and olefinic carbon; peak 5 corresponds to alcohol or ether carbon; peak 6 corresponds to methylene and methine carbon C (CH_2 and CH); peak 7 corresponds to methyl carbon C (CH_3).

(Figure 7). Both carbonyl ($\text{C}=\text{O}$) and carboxylic acid (COOH) moieties are partially reduced, forming new alcohol (C-OH) groups. It is, therefore, possible that the relatively intense (C-O) peak at 65 ppm in the Sutter's Mill IOM may have been formed through carbonyl and carboxyl C reduction during the processing that led to the IOM's overall molecular evolution.

Whereas alkali metal hydrides would certainly not have been present in parent body aqueous fluids, organic hydride donors could have been present. These include formic acid and pyruvic acid that have been detected in water extracts from Murchison (Cooper et al., 2011) and are powerful hydride donors via the oxidative decarboxylation reaction (March, 1992) to CO_2 and H_2 , and to acetate, CO_2 , and H_2 , respectively. The differences between PCA 91008's and Sutter's Mill's IOM (Figure 6) may then reflect differences in the reducing–oxidizing

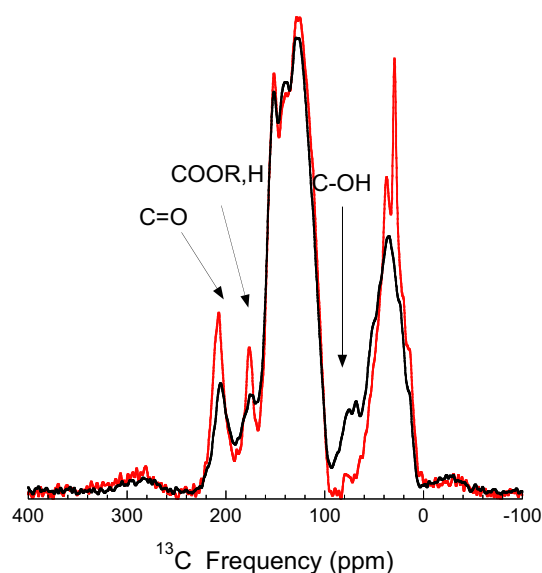


FIGURE 7. ^{13}C solid-state NMR of syn-IOM prepared from hydrocarbonization of glucose in water (250°C , 7 h; red spectrum) and after reaction with NaBH_4 (black spectrum). Partial reduction of aliphatic ketone (~ 210 ppm) and carboxyl carbon C (~ 175 ppm) to alcohol C (~ 65 ppm) is indicated. (Color figure can be viewed at wileyonlinelibrary.com)

potential of the fluids in which they were altered, provided that thermal alteration occurred under aqueous conditions.

The ^1H solid-state NMR spectra of IOM from Sutter's Mill, Tagish Lake "orig.," PCA 91008, and WIS 91600 provide insight into aromatic and aliphatic H (Figure 8). The fraction of aromatic H is an indicator of the degree of molecular evolution (Cody & Alexander, 2005; Herd et al., 2011). The ^1H -NMR spectra in Figure 8 are ordered in terms of the fraction of aromatic H (increasing from bottom to top). Whereas aromatic and aliphatic H are clearly distinguishable in Sutter's Mill's IOM, these are progressively less resolved (changing from a distinct peak for aliphatic H to a more subtle shoulder feature in the ^1H -NMR spectra, Figure 8) moving from Tagish Lake "orig." up to WIS 91600. The higher aromatic H in Sutter's Mill relative to Murchison's IOM supports the notion that it has been subjected to thermally derived molecular evolution.

The lack of resolution of the aromatic and aliphatic H peaks results from increased peak broadening (bottom to top) that is likely due to increased stable-free radical concentration (radicals are unpaired electrons bound to the organic macromolecule). Electron paramagnetic resonance (EPR) spectroscopy of IOM from the Tagish Lake clasts clearly shows that the number of stable-free radicals increases with increasing molecular evolution (Alexander et al., 2022). EPR spectroscopy of Sutter's Mill, PCA 91008, and WIS 91600 has not been performed, but from these ^1H -NMR spectra, it is

predicted that the number of free radicals (spins g^{-1}) would increase as follows: Sutter's Mill < Tagish Lake "orig" < PCA 91008 = WIS 91600. Note that $e^{-1}\text{H}$ interactions are much stronger than $e^{-13}\text{C}$ interactions ($\sim 4\times$) and will have a more obvious effect on ^1H -NMR spectra than on ^{13}C -NMR spectra.

Noble gases and labile element analysis help constrain the extent of alteration due to heating. From our analyses, it is clear that Sutter's Mill's IOM molecular structure is considerably evolved as compared to that in other CMs, for example, Murchison. This is also reflected in the lower noble gas concentrations and Ar/Xe and Kr/Xe ratios in Sutter's Mill IOM compared to Murchison IOM. Although there are no firm upper temperature estimates for alteration of the Tagish Lake "orig" IOM, hydrothermal alteration of the Murray CM chondrite's IOM at 300°C for 5 days yielded a highly aromatic molecular structure similar to that of Tagish Lake "orig" (Yabuta et al., 2007). PCA 91008 has experienced considerable loss of the volatile element Cd similar to that exhibited by Murchison after heating to 600°C for 1 week (Lipschutz et al., 1999), providing evidence that PCA 91008 was heated well above that of a typical CM. Similarities in molecular structure of WIS 91600 with PCA 91008 (shown here Figures 3a, 6 and 8) and in previous studies via ^{13}C solid-state NMR and pyrolysis gas chromatography–mass spectrometry (pyrGCMS; Yabuta et al., 2010) lead to the suggestion that WIS 91600 was also heated to significant temperatures.

It is noted that in the thermal metamorphism classification based on matrix mineralogy by Nakamura (2005), WIS 91600 is classified as Stage II (meaning phyllosilicates were transformed to hydrous glass) and PCA 91008 is classified as Stage III (meaning that small low crystalline secondary olivine was observed). Nakamura (2005) cites that Stage II corresponds to temperatures on the order of $300\text{--}500^\circ\text{C}$ (over a time-scale of 350 h) and Stage III corresponds to temperature on the order of $500\text{--}750^\circ\text{C}$. Nakamura (2005) recognized that kinetics must govern the times and temperatures to achieve a given stage. Finally, as to the source of heating, Nakamura (2005) excludes long-term radiogenic heating, acknowledged the possibility of impact heating, but ultimately concluded that the heating source remains undetermined. More recently, Quirico et al. (2018) favored rapid heating due to impacts through their analysis of Raman data on a large suite of IOM samples. There are likely other short-term heating scenarios that are equally plausible.

As to the details of the heating events, the abundance of N relative to C provides some valuable information (Foustoukos et al., 2021; Figure 9a,b). IOM from type 3 carbonaceous chondrites was heated for considerable time at moderate temperatures ($\sim 400\text{--}900^\circ\text{C}$ due to radiogenic parent body heating). In these samples, molecular

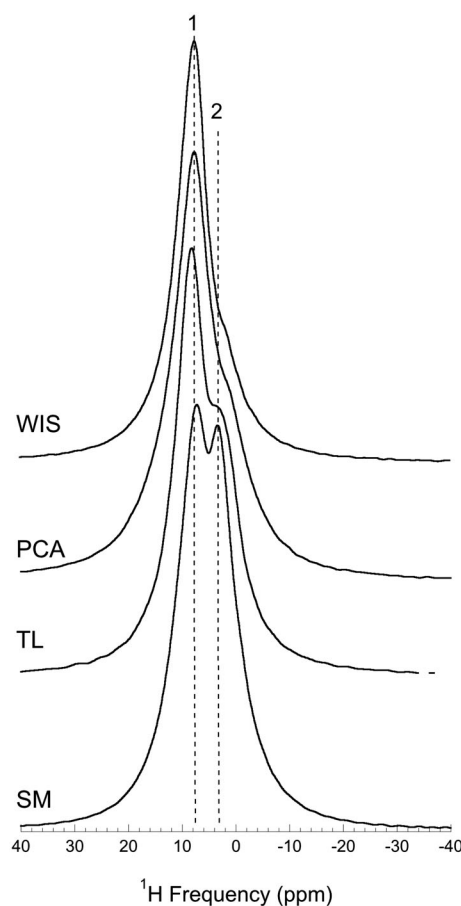


FIGURE 8. ^1H solid-state NMR of IOM derived from Sutter's Mill, Tagish Lake "orig" (Cody & Alexander, 2005), PCA 91008, and WIS 91600. Peak 1 corresponds to aromatic H (~ 7.5 ppm) and Peak 2 corresponds to aliphatic (CH_2 and CH) H (~ 3 ppm). There is systematic peak broadening apparent with Sutter's Mill < Tagish Lake "orig" < PCA 91008 = WIS 91600.

evolution (Cody et al., 2008) is accompanied by a considerable reduction of N/C (atom; Alexander et al., 2007; Figure 9b). For example, IOM isolated from Vigarano (CV3) has a molecular evolution temperature estimated (by intensity of the 1 s-sigma* exciton in the C-XANES spectra) to be $415 \pm 25^\circ\text{C}$ (Cody et al., 2008), assuming greater than a million years of radiogenic heating and a low N/C $\times 100$ of 0.8 (Alexander et al., 2007). The development of the 1 s-sigma* exciton has very sluggish kinetics, such that either very high temperatures or very long times are required (Cody et al., 2008). Subjecting IOM to high temperatures for short durations results in minimal to no reduction in N/C even up to high temperatures (Foustoukos et al., 2021; Okumura & Mimura, 2011). Longer term isothermal heating (60 + days) at more moderate temperatures results in greater N/C loss than with short duration heating (Foustoukos et al., 2021, Figure 9b).

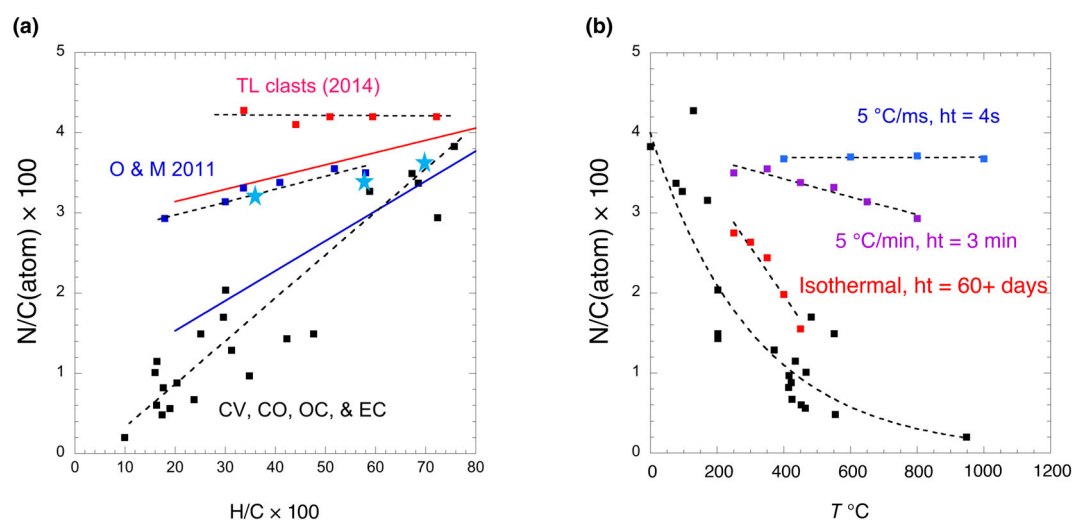


FIGURE 9. (a) $N/C \times 100$ plotted against $H/C \times 100$ for various IOM isolates from different meteorites, clasts from identical meteorites (Herd et al., 2011), and experimental thermal perturbation of IOM under different thermal regimes. Thermally evolved IOM from CV, CO, OC, and EC type 3+ meteorites (black squares), stepped pyrolysis of Murchison IOM (up to 800°C, Okumura & Mimura, 2011; blue squares), Tagish Lake Clasts (red squares), linear regressions from flash pyrolysis experiments (up to 1000°C, red line), long-term (250–400°C, 60+ days, Foustoukos et al., 2021) experiments on Murchison IOM (blue line), and Murchison a and b (this study), previously analyzed Murchison IOM (Alexander et al., 2007), and Sutter's Mill (this study) as pale blue stars. (b) $N/C \times 100$ versus temperature. Flash dry pyrolysis (5°C ms⁻¹ up to 1000°C) in blue squares (Foustoukos et al., 2021), stepped pyrolysis (5°C min⁻¹ up to 800°C) in purple squares (Okumura & Mimura, 2011), long-term hydrothermal processing (250–400°C for 60+ days) in red squares (Foustoukos et al., 2021), natural IOM isolated from type 3+ CV, CO, OC, and EC's (Alexander et al., 2007) with T estimates derived from 1 s-sigma* exciton intensity (Cody et al., 2008) indicating a strong time–temperature dependence on N/C reduction. Overall, significant differences in N/C and H/C molecular thermokinetics are indicated. (Color figure can be viewed at wileyonlinelibrary.com)

In Figure 9a $N/C \times 100$ is plotted against $H/C \times 100$, indicating that the kinetics of molecular evolution (exemplified by reduction of $H/C \times 100$) and N/C reduction are very different in different thermal regimes. The molecular evolution of Tagish Lake clasts resulted in minimal (if any) reduction in N/C , indicating a short duration moderate thermal event(s; Alexander et al., 2014; Herd et al., 2011; Figure 9a). Both PCA 91008 and WIS 91600 have N/C values similar to Murchison and other less molecularly evolved IOM (Alexander et al., 2007; Yabuta et al., 2010), suggesting that these meteorites also report short-duration thermal events (Foustoukos et al., 2021). Sutter's Mill's IOM has a N/C comparable to that of Murchison (Table 2) even though it is substantially molecularly evolved (lower H/C) relative to Murchison's IOM (Figures 1 and 4, Table 3), again indicating short-duration heating (Figure 9a). In Figure 9b, a relationship between heating time (duration) and temperature is evident with respect to the rate of $N/C \times 100$ reduction, indicating kinetic control. What event(s) caused such short-term heating (e.g., impact heating or some other short-duration event) is not clearly resolved but is likely similar among the Tagish Lake “orig,” PCA 91008, WIS 91600, and Sutter's Mill meteorites and differs from the long-term radiogenic thermal histories that modified the IOM in type 3 CV and

CO chondrites, ordinary chondrites, and enstatite chondrites (Figure 9a,b).

CONCLUSIONS

The principal results derived from this study are as follows. First, the time required to perform substantial analysis of IOM isolated from chondritic meteorites from the point of receiving a sample is predominantly governed by the time required for careful demineralization that at current state-of-the-art capabilities takes ~1 month, followed by parallel analyses where the maximum time is ~4 days, for ¹³C solid-state NMR, 1 day for ¹H solid-state NMR, a single sample EA-IRMS for H, C, and N elemental and isotopic abundances require 7 days; Raman and XRF spectroscopy require ~4 day per analysis (assuming a single sample and a single operator).

Second, our study shows that high-energy x-ray imaging results in no detectable beam-derived secondary electron damage, as determined by EA-IRMS or molecular (NMR, Raman, and FT-IR) spectroscopic and noble gas mass spectrometric methods. Any x-ray beam damage is below the levels of the detection of methods in the study.

Third, analysis of Murchison IOM from a different sample than analyzed previously (Alexander et al., 2007; Cody et al., 2002; Cody & Alexander, 2005) reveals statistically significant variation in the IOM molecular structure from a previous Murchison sample and variation in the molecular evolution of IOM from within a single meteorite. Similar and more extensive molecular evolution has been previously revealed in studies of clasts from the Tagish Lake meteorite (Alexander et al., 2014; Herd et al., 2011); discovery of such molecular variation in different Murchison samples suggests that it might be more general than previously recognized.

Fourth, careful analysis (elemental, isotopic, and molecular analysis, NMR, and Raman) of IOM isolated from Sutter's Mill reveals that this chondrite has been subjected to thermal modification that differs from that of type 3 chondrites (Figure 9a,b) that were subjected to long-term radiogenic heating; specifically, Sutter's Mill was subjected to higher temperature and shorter duration thermal perturbation from an undefined thermal process. Such fast thermal alteration has been concluded previously to explain the origin of heated CMs (e.g., Yabuta et al., 2010), and it may be more common than generally appreciated.

Acknowledgments—We gratefully acknowledge funding from NASA Emerging World grants 80NSSC20K0344, 80NSSC21K0654, and Solar System Workings grant 80NSSC19K0559. This work has also been supported by NASA under Award NNH09ZDA0070 and Contract NNM10AA11C issued through the New Frontiers Program, and Swiss SNF grant 51NF40 205606. We thank Tim McCoy, Curator of Meteorites at the Smithsonian National Museum of Natural History, for the Murchison meteorite sample used for this study, and Dolores Hill at the Lunar and Planetary Laboratory of the University of Arizona for providing the Sutter's Mill meteorite samples. Antarctic meteorite samples are recovered by the Antarctic Search for Meteorites (ANSMET) program, which has been funded by the NSF and NASA, and characterized and curated by the Department of Mineral Sciences of the Smithsonian Institution and the Astromaterials Curation Office at NASA Johnson Space Center. We are grateful to the OSIRIS-REx Sample Organics Analysis Working Group (SOAWG) for feedback on this work and to the entire OSIRIS-REx Team for making the return of samples from asteroid Bennu possible.

Data Availability Statement—The data are available at Zenodo public repository at www.zenodo.org.

Editorial Handling—Dr. A. J. Timothy Jull

REFERENCES

- Alexander, C. M. O'D. 2019. Quantitative Models for the Elemental and Isotopic Fractionation in Chondrites: The Carbonaceous Chondrites. *Geochimica et Cosmochimica Acta* 254: 277–309.
- Alexander, C. M. O'D., Bowden, R., Fogel, M. L., Howard, K. T., Herd, C. D. K., and Nittler, L. R. 2012. The Provenances of Asteroids, and their Contributions to the Volatile Inventories of the Terrestrial Planets. *Science* 337: 721–23.
- Alexander, C. M. O. D., Cody, G. D., De Gregorio, B. T., Nittler, L. R., and Stroud, R. M. 2017. The Nature, Origin and Modification of Insoluble Organic Matter in Chondrites, the Major Source of Earth's C and N. *Chemie der Erde—Geochemistry* 77: 227–256.
- Alexander, C. M. O'D., Cody, G. D., Kebukawa, Y., Bowden, R., Fogel, M. L., Kilcoyne, A. L. D., Nittler, L. R., and Herd, C. D. K. 2014. Elemental, Isotopic and Structural Changes in Tagish Lake Insoluble Organic Matter Produced by Parent Body Processes. *Meteoritics & Planetary Science* 49: 503–525.
- Alexander, C. M. O'D., Fogel, M., Yabuta, H., and Cody, G. D. 2007. The Origin and Evolution of Chondrites Recorded in the Elemental and Isotopic Compositions of their Macromolecular Organic Matter. *Geochimica et Cosmochimica Acta* 71: 4380–4403.
- Alexander, C. M. O'D., Howard, K., Bowden, R., and Fogel, M. L. 2013. The Classification of CM and CR Chondrites Using Bulk H, C and N Abundances and Isotopic Compositions. *Geochimica et Cosmochimica Acta* 123: 244–260.
- Alexander, C. M. O'D., Nilges, M. J., Cody, G. D., and Herd, C. D. K. 2022. Are Radicals Responsible for the Variable Deuterium Enrichments in Chondritic Insoluble Organic Material? *Geochimica et Cosmochimica Acta* 316: 135–149.
- Alexander, C. M. O'D., and Pizzarello, S. 2015. Carbonaceous Chondrites, Organic Chemistry of. In *Encyclopedia of Astrobiology*, edited by M. Gargaud, W. M. Irvine, R. Amils, H. J. Cleaves, D. L. Pinti, J. C. Quintanilla, D. Rouan, T. Spohn, S. Tirard, and M. Viso, 374–76. Berlin Heidelberg, Berlin, Heidelberg: Springer.
- Beck, P., Quirico, E., Garenne, A., Yin, Q. Z., Bonal, L., Schmitt, B., Montes-Hernandez, G., Montagnac, G., Chiriach, R., and Toche, F. 2014. The Secondary History of Sutter's Mill CM Carbonaceous Chondrite Based on Water Abundance and the Structure of its Organic Matter from Two Clasts. *Meteoritics & Planetary Science* 49: 2064–73.
- Beysac, O., Goffe, B., Chopin, C., and Rouzaud, J. N. 2002. Raman Spectra of Carbonaceous Material in Metasediments: A New Geothermometer. *Journal of Metamorphic Petrology* 20: 859–871.
- Bonal, L., Quirico, E., Flandinet, L., and Montagnac, G. 2016. Thermal History of Type 3 Chondrites from the Antarctic Meteorite Collection Determined by Raman Spectroscopy of their Polyaromatic Carbonaceous Matter. *Geochimica et Cosmochimica Acta* 189: 312–337.
- Braukmüller, N., Wombacher, F., Hezel, D. C., Escoube, R., and Münker, C. 2018. The Chemical Composition of Carbonaceous Chondrites: Implications for Volatile Element Depletion, Complementarity and Alteration. *Geochimica et Cosmochimica Acta* 239: 17–48.

- Busemann, H., Alexander, C. M. O'D., and Nittler, L. R. 2007. Characterization of Insoluble Organic Matter in Primitive Meteorites by MicroRaman Spectroscopy. *Meteoritics & Planetary Science* 42: 1387–1416.
- Busemann, H., Alexander, C. M. O'D., Nittler, L. R., and Wieler, R. 2008. Noble Gases in Insoluble Organic Matter in the Very Primitive Meteorites Bells, EET 92042 and GRO 95577. 39th Lunar and Planetary Science Conference, abstract #1777.
- Busemann, H., Baur, H., and Wieler, R. 2000. Primordial Noble Gases in "Phase Q" in Carbonaceous and Ordinary Chondrites Studied by Closed System Stepped Etching. *Meteoritics & Planetary Science* 35: 949–973.
- Cody, G. D., and Alexander, C. M. O'D. 2005. NMR Studies of Chemical Structural Variation of Insoluble Organic Matter from Different Carbonaceous Chondrite Groups. *Geochimica et Cosmochimica Acta* 69: 1085–97.
- Cody, G. D., Alexander, C. M. O'D., and Tera, F. 2002. Solid State (^1H and ^{13}C) NMR Spectroscopy of the Insoluble Organic Residue in the Murchison Meteorite: A Self-Consistent Quantitative Analysis. *Geochimica et Cosmochimica Acta* 66: 1851–65.
- Cody, G. D., Alexander, C. M. O'D., Yabuta, H., Kilcoyne, A. L. D., Araki, T., Ade, H., Dera, P., Fogel, M., Miltzer, B., and Mysen, B. O. 2008. Organic Thermometry for Chondritic Parent Bodies. *Earth and Planetary Science Letters* 272: 446–455.
- Cody, G. D., Brandes, J., Jacobsen, C., and Wirick, S. 2009. Soft X-Ray Induced Chemical Modification of Polysaccharides in Vascular Plant Cell Walls. *Journal of Electron Spectroscopy and Related Phenomena* 170: 57–64.
- Cody, G. D., Heying, E., Alexander, C. M. O'D., Nittler, L. R., Kilcoyne, A. L. D., Sandford, S. A., and Stroud, R. M. 2011. Establishing a Molecular Relationship Between Chondritic and Cometary Organic Solids. *Proceedings of the National Academy of Sciences of the United States of America* 108: 19171–76.
- Cooper, G., Reed, C., Nguyen, D., Carter, M., and Wang, Y. 2011. Detection and Formation Scenario of Citric Acid, Pyruvic Acid, and Other Possible Metabolism Precursors in Carbonaceous Meteorites. *Proceedings of the National Academy of Sciences of the United States of America* 108: 14015–20.
- Foustoukos, D. I. 2012. Metastable Equilibrium in the C-H-O System: Graphite Deposition in Crustal Fluids. *American Mineralogist* 97: 1373–80.
- Foustoukos, D. I., Alexander, C. M. O'D., and Cody, G. D. 2021. H and N Systematics in Thermally Altered Chondritic Insoluble Organic Matter: An Experimental Study. *Geochimica et Cosmochimica Acta* 300: 44–64.
- Gardinier, A., Derenne, S., Robert, F., Behar, F., Largeau, C., and Maquet, J. 2000. Solid State CP/MAS ^{13}C NMR of the Insoluble Matter of the Orgueil and Murchison Meteorites: Quantitative Study. *Earth and Planetary Science Letters* 184: 9–21.
- Glavin, D. P., Alexander, C. M. O'D., Aponte, J. C., Dworkin, J. P., Elsila, J. E., and Yabuta, H. 2018. The Origin and Evolution of Organic Matter in Carbonaceous Chondrites and Links to their Parent Bodies. In *Primitive Meteorites and Asteroids*, edited by N. Abreu, 205–271. Amsterdam, the Netherlands: Elsevier.
- Glavin, D. P., Eckley, S. A., Aponte, J. A., Berger, E. L., Burton, A. S., Dworkin, J. P., Elsila, J. E., et al. (2023). Investigating the Impact of X-Ray Computed Tomography Imaging on Soluble Organic Matter in the Murchison Meteorite: Implications for Benu Sample Analyses. *Meteoritics & Planetary Science*.
- Guice, G. L., Ackerson, M. R., Holder, R. M., George, F. R., Browning-Hanson, J. F., Burgess, J. L., Foustoukos, D. I., Becker, H. A., Nelson, W. R., and Viète, D. R. 2021. Suprasubduction Zone Ophiolite Fragments in the Central Appalachian Orogen: Evidence for Mantle and Moho in the Baltimore Mafic Complex (Maryland, USA). *Geospheres* 17. <https://doi.org/10.1130/GES02289.1>
- Hamilton, V. E., Simon, A. A., Christensen, P. R., Reuter, D. C., Clark, B. E., Barucci, M. A., Bowles, N. E., et al. 2019. Evidence for Widespread Hydrated Minerals on Asteroid (101955) Benu. *Nature Astronomy* 3: 332–340.
- Herd, C. D. K., Blinova, A., Simkus, D. N., Huang, Y., Tarozo, R., Alexander, C. M. O'D., Gyngard, F., et al. 2011. Origin and Evolution of Prebiotic Organic Matter as Inferred from the Tagish Lake Meteorite. *Science* 332: 1304–7.
- Homma, Y., Kouketsu, Y., Kagi, H., Mikouchi, T., and Yabuta, H. 2015. Raman Spectroscopic Thermometry of Carbonaceous Material in Chondrites: Four-Band Fitting Analysis and Expansion of Lower Temperature Limit. *Journal of Mineralogical and Petrological Sciences* 110: 276–282.
- Jenniskens, P., Fries, M. D., Yin, Q.-Z., Zolensky, M., Krot, A. N., Sandford, S. A., Sears, D., et al. 2012. Radar-Enabled Recovery of the Sutter's Mill Meteorite, a Carbonaceous Chondrite Regolith Breccia. *Science* 338: 1583–87.
- Kallemeyn, G. W., and Wasson, J. T. 1981. The Compositional Classification of Chondrites. I—The Carbonaceous Chondrite Groups. *Geochimica et Cosmochimica Acta* 45: 1217–30.
- Kebukawa, Y., and Cody, G. D. 2015. A Kinetic Study of the Formation of Organic Solids from Formaldehyde: Implications for the Origin of Extraterrestrial Organic Solids in Primitive Solar System Objects. *Icarus* 248: 412–423.
- Kebukawa, Y., Kilcoyne, A. L. D., and Cody, G. D. 2013. Exploring the Potential Formation of Organic Solids in Chondrites and Comets through Polymerization of Interstellar Formaldehyde. *The Astrophysical Journal* 771: 19.
- Lewis, R. S., Srinivasan, B., and Anders, E. 1975. Host Phase of a Strange Xenon Component in Allende. *Science* 190: 1251–62.
- Lipschutz, M. E., Zolensky, M. E., and Bell, M. S. 1999. New Petrographic and Trace Element Data on Thermally Metamorphosed Carbonaceous Chondrites. *Antarctic Meteorite Research* 12: 57–80.
- Long, D. A. 1977. *Raman Spectroscopy*. New York: McGraw-Hill.
- March, J. 1992. *Advanced Organic Chemistry*. New York: Wiley-Interscience.
- Munoz Caro, G. M., Matrajt, G., Dartois, E., Nuevo, M., d'Hendcourt, L., Deboffe, D., Montagnac, G., Chauvin, N., Boukari, C., and Le Du, D. 2006. Nature and Evolution of the Dominant Carbonaceous Matter in Interplanetary Dust Particles: Effects of Irradiation and Identification with a Type of Amorphous Carbon. *Astronomy and Astrophysics* 459: 147–159.
- Nakamura, T. 2005. Post-Hydration Thermal Metamorphism of Carbonaceous Chondrites. *Journal of Mineralogical and Petrological Sciences* 100: 260–272.

- Oba, Y., and Naraoka, H. 2009. Elemental and Isotopic Behavior of Macromolecular Organic Matter from CM Chondrites during Hydrous Pyrolysis. *Meteoritics & Planetary Science* 44: 943–954.
- Okumura, F., and Mimura, K. 2011. Gradual and Stepwise Pyrolyses of Insoluble Organic Matter from the Murchison Meteorite Revealing Chemical Structure and Isotopic Distribution. *Geochimica et Cosmochimica Acta* 75: 7063–80.
- Ott, U. 2014. Planetary and Pre-Solar Noble Gases in Meteorites. *Chemie der Erde—Geochemistry* 74: 519–544.
- Pasteris, J. D., and Chou, I. M. 1998. Fluid-Deposited Graphitic Inclusions in Quartz: Comparison between KTB (German Continental Deep-Drilling) Core Samples and Artificially Reequilibrated Natural Inclusions. *Geochimica et Cosmochimica Acta* 62: 109–122.
- Pasteris, J. D., and Wopenka, B. 1991. Raman Spectra of Graphite as Indicators of Degree of Metamorphism. *Canadian Mineralogist* 29: 1–9.
- Pizzarello, S., Davidowski, S. K., Holland, G. P., and Williams, L. B. 2013. Processing of Meteoritic Organic Materials as a Possible Analog of Early Molecular Evolution in Planetary Environments. *Proceedings of the National Academy of Science of the United States of America* 110: 15614–19.
- Potiszil, C., Montgomery, W., and Sephton, M. A. 2021. Heterogeneity within Refractory Organic Matter from CM2 Carbonaceous Chondrites: Evidence from Raman Spectroscopy. *Earth and Planetary Science Letters* 574: 117149.
- Pretsch, E., Bühlmann, P., and Affolter, C. 2000. *Structure Determination of Organic Compounds*. New York: Springer.
- Quirico, E., Bonal, L., Beck, P., Alexander, C. M. O'D., Yabuta, H., Nakamura, T., Nakato, A., et al. 2018. Prevalence and Nature of Heating Processes in CM and C2-Ungrouped Chondrites as Revealed by Insoluble Organic Matter. *Geochimica et Cosmochimica Acta* 241: 17–37.
- Quirico, E., Orthous-Dauny, F.-R., Beck, P., Bonal, L., Brunetto, R., Dartois, E., Pino, T., et al. 2014. Origin of insoluble matter in type 1 and 2 chondrites: New clues, new questions. *Geochemical and Cosmochemical Journal* 136: 80–99.
- Riebe, M. E. I., Busemann, H., Wieler, R., and Maden, C. 2017. Closed System Step Etching of CI Chondrite Ivuna Reveals Primordial Noble Gases in the HF-Solubles. *Geochimica et Cosmochimica Acta* 205: 65–83.
- Rotundi, A., Baratta, G. A., Borg, J., Brucato, J. R., Busemann, H., Colangeli, L., D'Hendecourt, L., et al. 2008. Combined Micro-Raman, Micro-Infrared, and Field Emission Scanning Electron Microscope Analyses of Comet 81P/Wild 2 Particles Collected by Stardust. *Meteoritics & Planetary Science* 43: 367–397.
- Sessions, A. L. 2001. *Hydrogen Isotope Ratios of Individual Organic Compounds*. Indiana: Indiana University.
- Smith, J. W., and Kaplan, I. R. 1970. Endogenous Carbon in Carbonaceous Meteorites. *Science* 167: 1367–70.
- Spring, N., Busemann, H., Vogel, N., Huber, L., Wieler, R., Maden, C., and Alexander, C. M. O'D. 2011. The Susceptibility of Phase Q to Pyridine: Are CI Chondrites Unique? *Meteoritics & Planetary Science Supplement* 74: 5527.
- Srinivasan, B. 1977. Noble Gases in Six Ordinary Chondrites: Comparison of Exposure Ages from Noble Gases with ²⁶Al Ages. *Geochimica et Cosmochimica Acta* 41: 977–983.
- Starkey, N. A., Franchi, I. A., and Alexander, C. M. O'D. 2013. A Raman Spectroscopic Study of Organic Matter in Interplanetary Dust Particles and Meteorites Using Multiple Wavelength Laser Excitation. *Meteoritics & Planetary Science* 48: 1800–1822.
- Steele, A., Benning, L. G., Wirth, R., Siljeström, S., Fries, M. D., Hauri, E., Conrad, P. G., et al. 2018. Organic Synthesis on Mars by Electrochemical Reduction of CO₂. *Science Advances* 4: eaat5118.
- Visser, R., John, T., Menneken, M., Patzek, M., and Bischoff, A. 2018. Temperature Constraints by Raman Spectroscopy of Organic Matter in Volatile-Rich Clasts and Carbonaceous Chondrites. *Geochimica et Cosmochimica Acta* 241: 38–55.
- Wieler, R., Anders, E., Baur, H., Lewis, R. S., and Signer, P. 1992. Characterisation of Q-Gases and Other Noble Gas Components in the Murchison Meteorite. *Geochimica et Cosmochimica Acta* 56: 2907–21.
- Wolf, D., and Palme, H. 2001. The Solar System Abundances of Phosphorus and Titanium and the Nebular Volatility of Phosphorus. *Meteoritics & Planetary Science* 36: 559–571.
- Wopenka, B., and Pasteris, J. D. 1993. Structural Characterization of Kerogens to Granulite-Facies Graphite—Applicability of Raman Microprobe Spectroscopy. *American Mineralogist* 78: 533–557.
- Yabuta, H., Alexander, C. M. O'D., Fogel, M. L., Kilcoyne, A. L. D., and Cody, G. D. 2010. A Molecular and Isotopic Study of the Macromolecular Organic Matter of the Ungrouped C2 WIS 91600 and its Relationship to Tagish Lake and PCA 91008. *Meteoritics & Planetary Science* 45: 1446–60.
- Yabuta, H., Williams, L. B., Cody, G. D., Alexander, C. M. O'D., and Pizzarello, S. 2007. The Insoluble Carbonaceous Material of CM Chondrites: A Possible Source of Discrete Organic Compounds under Hydrothermal Conditions. *Meteoritics & Planetary Science* 42: 37–48.
- Zhu, W., Li, X., Sun, R., Yan, Y., Liu, J., Wang, Z., and Yu, X. 2023. Microstructural Evolution of Coal to Char after Pyrolysis Using Laser-Induced Breakdown Spectroscopy and Raman Spectroscopy. *Energy* 267: 126558.
- Zinner, E. 2014. Presolar Grains. In *Meteorites and Cosmochemical Processes*, edited by A. M. Davis, 181–213. Oxford: Elsevier.